Sessile alveolar macrophage connexin-43 determines mechano-immunity in the lung

Liberty Mthunzi[1], Galina A Gusarova[1], Mohammad N Islam[1], Sunita Bhattacharya[1], Jahar Bhattacharya[1]

[1]Lung Biology Laboratory, Division of Pulmonary Allergy and Critical Care, Department of Medicine, Vagelos College of Physicians and Surgeons, Columbia University, New York, NY 10032

*Correspondence to: jb39@cumc.columbia.edu

Abstract

Although lung immunity is pathogen induced, the immunity can also be induced by mechanical distortion of the lung. The causal basis of the lung's mechanosensitive immunity remains unclear. Here, through live optical imaging of mouse lungs, we show that alveolar stretch due to hyperinflation induced prolonged cytosolic Ca^{2+} increases in sessile alveolar macrophages (AMs). Knockout studies revealed that the Ca^{2+} increases resulted from Ca^{2+} diffusion from the alveolar epithelium to sessile AMs through connexin 43 (Cx43)-containing gap junctions. Lung inflammation and injury in mice exposed to injurious mechanical ventilation were inhibited by AM-specific Cx43 knockout, or AM-specific delivery of a calcium inhibitor. We conclude, Cx43 gap junctions and calcium mobilization in sessile AMs determine the lung's mechanosensitive immunity, providing a therapeutic strategy against hyperinflation-induced lung injury.

Keywords

Sessile alveolar macrophage, connexin-43, mechano-immunity, calcium, live microscopy, mechanical ventilation, tumor necrosis factor alpha (TNFα)

Introduction

The lung's innate immune response underlies acute lung injury (ALI), in which failure of the lung's air-blood barrier leads to pulmonary edema, hence hypoxemia, a proximate cause of the high mortality associated with the acute respiratory distress syndrome (ARDS) (*1*). Receptors that sense pathogen-associated molecular patterns (PAMPs) initiate the immunity. Thus, inhaled endotoxin ligates toll-like receptor 4 (TLR4), a PAMP expressed by alveolus-adherent, sessile AMs, leading to a cytokine-induced immune response (*2*). Despite this understanding, what is puzzling is that the immune response can also be mechanosensitive, in that it is induced by mechanical distortions such as alveolar stretch in a pathogen-independent manner that seemingly bypasses the PAMP mechanism (*3, 4*). This is evident in lungs undergoing hyperinflation, a condition associated with alveolar stretch, by mechanical ventilation in the absence of lung infection (*5, 6*), or after strenuous exercise (*7, 8*). However, the cause of the mechanosensitive immunity is not clear.

Mechanosensitive cell signaling has been understood in terms of mechanosensory ion channels such as TRPV4 and Piezo 1 (*9-11*). A role for macrophage TRPV4 is proposed as a mechanism for VILI (*12*). Evidence *in vitro* indicates that mechanical perturbations cause Ca^{2+} entry through Piezo 1 channels in bone marrow-derived macrophages (BMDMs) (*11*), and secretion of the proinflammatory cytokine, tumor necrosis factor-alpha (TNFα) in AMs (*13*). These findings are the basis of the proposal that alveolar hyperinflation stretches alveolar macrophages, resulting in the lung's mechanosensitive immunity leading to lung injury (*14*). However, this macrophage-stretch hypothesis remains untested *in situ*.

Real-time confocal microscopy (RCM) of the live mouse lung provided an opportunity to test the macrophage-stretch hypothesis in intact alveoli (*2*). RCM revealed the alveolar epithelium by the fluorescence of the cytosolic localizing dye, calcein, which demarcated the non-fluorescent air space of the alveolar lumen. Sessile AMs, that constitute the majority of resident myeloid cells of the alveolar lumen, were phenotypically identified as alveolus adherent, lumen protruding cells that expressed fluorescence of GFP-linked CD11c, and immunofluorescence of the AM marker, SiglecF (*2*).

Results

Sessile AMs are protected against shape changes during lung hyperinflation

We considered that the close apposition of sessile AMs to the alveolar epithelium might cause sufficient mechanical coupling to coordinate stretch responses in these cell types. We tested this hypothesis by assessing cell shape changes using our previously reported approach, in which we superimpose differently pseudocolored images of a single alveolus obtained at different alveolar inflation pressures (*15*). Thus, lung expansion causes merge, or separation of the pseudocolors at respectively, non-distending or distending segments of the alveolus. Here, we affirmed that increasing the lung's inflation pressure from a baseline of 5 to 15 cmH_2O, induced asymmetric alveolar stretch in that distension was evident in some but not all septal segments within the same alveolus (**Fig. 1a**). Our new finding was that sessile AMs were almost exclusively located at the meeting points of adjacent septa, the so called alveolar corners (*15*), at which distension was notably absent (**Fig. 1a, b**). Accordingly, the pseudocolor

superimposition approach, applied to differently colored images obtained during hyperinflation and baseline, revealed a near perfect merge of the pseudocolors for sessile AMs (**Fig. 1c**), indicating that the AMs did not undergo shape changes during hyperinflation.

To pursue the shape change question further, we stained sessile AMs with SiglecF fluorescence to mark the cell perimeter. Then we imaged single AMs by RCM in a series of 1.7-micron thick optical sections taken along the depth axis from the pleural plane to the plane of the alveolar lumen. As depicted in the example shown (**Fig. 1d**), this serial imaging revealed AM sphericity in that at a depth of ~7 to ~14 microns, comprising the major part of the cell body, the cross-sectional profile was circular. After hyperinflation, not only was the circular cross-section retained, but the cross-sectional diameters at each of the optical levels were identical, indicating that hyperinflation did not modify the sphericity or the cross-sectional diameters of sessile AMs. Taken together, our data fail to confirm that alveolar hyperinflation causes change of AM shape as a critical immunogenic mechanism.

Hyperinflation mobilizes calcium in a subset of sessile AMs

An increase in the cytosolic Ca^{2+} (cCa^{2+}) signals immune initiation in alveoli (*2, 16*). In lungs exposed to LPS, about 40% of sessile AMs communicate cCa^{2+} spikes to the alveolar epithelium through connexin43 (Cx43)-containing gap junctions (*2*). Although alveolar stretch due to hyperinflation activates cCa^{2+} waves in the alveolar epithelium (*17*), it is not known whether the waves travel to sessile AMs across gap junctions. To test this possibility, we induced transient hyperinflation by increasing the inflation pressure to 15 cmH_2O for 15 seconds, then returning the pressure to baseline of 5 cmH_2O. Within 5 minutes, cCa^{2+} increase initiated in some sessile AMs, reaching peak in ~20 minutes, then subsiding to baseline in a further 10 minutes (**Fig**. **2a**). Concomitantly, in the adjoining alveolar epithelium cCa^{2+} oscillations increased, although mean cCa^{2+} remained unchanged (**sFig. 3**). Overall, we detected the cCa^{2+} increases in 35% of AMs, since several AMs in adjoining alveoli that were also subjected to the stretching effect of hyperinflation failed to show cCa^{2+} increases (**Fig. 2b**). In separate experiments, we confirmed the hyperinflation-induced cCa^{2+} increase in AMs, then we gave alveolar microinfusion of xestospongin C (XeC), which inhibits store release of Ca^{2+} (*18*). In every instance, XeC blocked the induced cCa^{2+} increase (**Fig. 2c**), indicating that Ca^{2+} release from intracellular stores of AMs was responsible for the Ca^{2+} increases. These findings indicate that despite the absence of shape changes, hyperinflation activated a definitive cCa^{2+} increase in a subset of sessile AMs.

Connexin-43 determines calcium mobilization in sessile AMs

To determine mechanisms, we considered the role of gap junctional communication (GJC) between sessile AMs and the alveolar epithelium as underlying the AM cCa^{2+} response. We tested this hypothesis by quantifying GJC in sessile AMs in terms of fluorescence recovery after photobleaching (FRAP), in which fluorescence recovery signifies communication between adjoining cells (*2*). Thus, we first identified AMs that did or did not respond with cCa^{2+} increases following hyperinflation. Then we determined the extent of GJC in responding and non-

responding AMs in terms of the fluorescence recovery. Our findings indicate that GJC varied amongst the responders, but that the variability correlated positively with the extent of the cCa^{2+} increase above baseline (**Fig. 2d**). Notably, we detected no cCa^{2+} increases in AMs in which fluorescence recovery was less than 20% of pre-bleach values, indicating that robust GJC was required to elicit the cCa^{2+} increases. Further, in affirmation of our reported findings (*2*), transgenic mice lacking Cx43 specifically in sessile AMs ($Cx43^{KO}$) lacked GJC between the AMs and the epithelium (*2*) (**sFig. 4**). The hyperinflation-induced cCa^{2+} increase was markedly inhibited in sessile AMs of $Cx43^{KO}$ mice than of littermate controls ($Cx43^{FL}$) (**Fig. 2e**). Together, these findings indicated that epithelium-AM communication through Cx43-containing GJCs determined the hyperinflation-induced cCa^{2+} increases in sessile AMs.

Mechanosensitive TNFα secretion occurs in a subset of sessile AMs

Although it is understood that secretion of proinflammatory cytokines drives lung immunity, mechanisms linking mechanical tissue stress and cytokine secretion remain unclear. Importantly, understanding is lacking as to the cellular origins of cytokines secreted in the bronchoalveolar lavage (BAL) after ventilation at high tidal volume (*19, 20*). Depletion of AMs by clodronate treatment decreases the BAL cytokine levels (*21, 22*), suggesting AMs are the cytokine source. However, not understood is the extent to which AM interactions with neighboring cells determine the secretion. Here, we considered these issues in relation to AM secretion of the cytokine tumor necrosis factor alpha (TNFα). We expressed fluorescent TNFα in AMs by intranasal instillation of liposome complexed GFP-TNFα plasmid. At baseline, TNFα fluorescence was well expressed in all AMs imaged (**sFig. 5**). However, although hyperinflation decreased TNFα fluorescence in a time course of minutes (**Fig. 3a**), the extent of the secretion response varied considerably between individual AMs. To determine mechanisms, we carried out FRAP to detect efficiency of GJC in each AM. Linear regression analysis revealed a strong correlation between the efficacy of GJC and the secretory response (**Fig. 3b**). Thus, our determinations of TNFα secretion and GJC on a single cell basis revealed that GJC between AMs and the epithelium was a critical determinant of the secretion.

Following secretion in the alveolar lumen, TNFα proinflammatory effects are attributable to ligation of the TNFα receptor-1 (TNFR1) expressed on the alveolar epithelium. The ligation, which is critical for the lung's subsequent immune response, causes TNFR1's ectodomain shedding (*23*), a response that occurs following hyperinflation (*24*). Here, the hyperinflation-induced TNFR1 shedding was inhibited in $Cx43^{KO}$ mice (**Fig. 3c**), pointing to the critical role played by Cx43-containing GJCs in the proinflammatory effect of alveolar stretch. Thus, gap junction-based interactions between sessile AMs and the adjoining epithelium were critical for the mechanosensitive proinflammatory response to hyperinflation.

Inhibition of sessile AM calcium mobilization protects against ventilator-induced lung injury

The mouse model for VILI (*25*) provided an opportunity to determine whether GJC between the alveolar epithelium and AMs was responsible for the lung inflammation that leads to VILI.

Hence, we mechanically ventilated $Cx43^{FL}$ and $Cx43^{KO}$ mice at low (LTV), or high (HTV) tidal volume for 2 hours. Subsequently, we assayed the bronchoalveolar lavage (BAL) for neutrophil and cytokine levels to quantify lung inflammation (**Fig. 4a, c**), and protein levels to quantify lung injury (**Fig. 4b**). These assays indicated that although HTV ventilation increased lung inflammation and barrier injury in $Cx43^{FL}$ mice, both responses were markedly diminished in $Cx43^{KO}$ mice. Thus, our findings indicate that the presence of Cx43, hence gap junctional channels in sessile AMs was critical for HTV-induced cytokine signaling and lung injury.

These findings motivated us to consider a macrophage-targeted therapeutic approach that might block the hyperinflation-induced cCa^{2+} increase in sessile AMs, thereby inhibiting subsequent proinflammatory signaling. Since AMs engulf surfactant from the alveolar space, drug delivery in surfactant vehicle provides an AM-targeted therapeutic approach (*26*). However, since the efficacy of AM-targeted delivery has not been directly confirmed, we intranasally instilled fluorescent surfactant (FS) alone, or FS in suspension with liposomes encapsulating rhodamine-B labelled dextran 70kDa (FS-lip). RCM images indicated that for both FS and FS-lip instillations, fluorescence uptake occurred predominantly in sessile AMs (**Fig. 5a, b**). Further, flow cytometry of cells derived from lung digests indicated that FS-lip was evident predominantly in AM fractions (**sFig. 6b**). These findings indicated that given together with surfactant, airway instilled liposomes targeted sessile AMs. Accordingly, intranasal instillation of FS-lip, in which the liposomes encapsulated xestospongin C resulted in marked reduction of hyperinflation-induced cCa^{2+} increase in sessile AMs (**Fig. 5c**). Concomitantly, the xestospongin C containing FS-lip instillation markedly diminished the BAL markers of lung inflammation and lung injury (**Fig. 5d-f**). Hence, inhibition of hyperinflation-induced cCa^{2+} increases in sessile AMs inhibited VILI.

Conclusions

Conclusions to be drawn from our present findings are first, that the directionality and duration of GJC dependent Ca^{2+} signaling between sessile AMs and the alveolar epithelium impact immune outcomes in the lung. Previously, we reported that 24 hours after lung exposure to inhaled LPS, sessile AMs induced brief cCa^{2+} spikes, lasting a few seconds that travel by Cx43-dependent GJC from the AMs to the alveolar epithelium to suppress inflammation (*2*). Thus, AM-specific Cx43 deletion inhibits the GJC and worsens LPS-induced lung injury. In present studies, we failed to find any evidence of short-lived cCa^{2+} spikes in sessile AMs. By contrast, in response to hyperinflation, cCa^{2+} waves travelled retrogradely from epithelium to AM, and they were of prolonged duration, lasting more than 20 minutes. Evidently, the duration of the hyperinflation-induced cCa^{2+} increase was sufficient to induce TNFa secretion, thereby initiating the extensive cytokine response underlying lung inflammation and injury. Since the proinflammatory cytokine response was inhibited by Cx43 deletion in sessile AMs, we conclude that AM-epithelium GJC played a critical mechanistic role in VILI.

Second, we achieved macrophage-targeted therapy to suppress AM cCa^{2+} increases that lead to the barrier damaging lung immune response underlying VILI. Thus, the Ca^{2+} inhibitor, xestospongin C was safely delivered to AMs in liposomes suspended in surfactant. Since all mice survived the therapeutic instillation, we interpret that bystander side effects that could

threaten survival were entirely absent. Since the liposome-based delivery occurred predominantly to AMs, we may rule out a role for dendritic cells in the hyperinflation-induced immune response. To the extent that macrophage cCa^{2+} increases initiate pathogenic signaling for multiple diseases in the lung, the application of the present therapeutic approach requires consideration in other disease settings.

References

1. M. A. Matthay *et al.*, Acute respiratory distress syndrome. *Nat Rev Dis Primers* **5**, 18 (2019).
2. K. Westphalen *et al.*, Sessile alveolar macrophages communicate with alveolar epithelium to modulate immunity. *Nature* **506**, 503-506 (2014).
3. H. H. Webb, D. F. Tierney, Experimental pulmonary edema due to intermittent positive pressure ventilation with high inflation pressures. Protection by positive end-expiratory pressure. *Am Rev Respir Dis* **110**, 556-565 (1974).
4. L. A. Hernandez, K. J. Peevy, A. A. Moise, J. C. Parker, Chest wall restriction limits high airway pressure-induced lung injury in young rabbits. *J Appl Physiol (1985)* **66**, 2364-2368 (1989).
5. O. Gajic *et al.*, Ventilator-associated lung injury in patients without acute lung injury at the onset of mechanical ventilation. *Crit Care Med* **32**, 1817-1824 (2004).
6. R. Pinheiro de Oliveira, M. P. Hetzel, M. dos Anjos Silva, D. Dallegrave, G. Friedman, Mechanical ventilation with high tidal volume induces inflammation in patients without lung disease. *Crit Care* **14**, R39 (2010).
7. S. R. Hopkins *et al.*, Intense exercise impairs the integrity of the pulmonary blood-gas barrier in elite athletes. *Am J Respir Crit Care Med* **155**, 1090-1094 (1997).
8. S. R. Hopkins, R. B. Schoene, W. R. Henderson, R. G. Spragg, J. B. West, Sustained submaximal exercise does not alter the integrity of the lung blood-gas barrier in elite athletes. *J Appl Physiol (1985)* **84**, 1185-1189 (1998).
9. A. G. Solis *et al.*, Mechanosensation of cyclical force by PIEZO1 is essential for innate immunity. *Nature* **573**, 69-74 (2019).
10. K. Hamanaka *et al.*, TRPV4 initiates the acute calcium-dependent permeability increase during ventilator-induced lung injury in isolated mouse lungs. *Am J Physiol Lung Cell Mol Physiol* **293**, L923-932 (2007).
11. H. Xu *et al.*, Mechanical force modulates macrophage proliferation via Piezo1-AKT-Cyclin D1 axis. *Faseb j* **36**, e22423 (2022).
12. K. Hamanaka *et al.*, TRPV4 channels augment macrophage activation and ventilator-induced lung injury. *Am J Physiol Lung Cell Mol Physiol* **299**, L353-362 (2010).
13. J. Pugin *et al.*, Activation of human macrophages by mechanical ventilation in vitro. *Am J Physiol* **275**, L1040-1050 (1998).
14. E. M. Orsini *et al.*, Stretching the Function of Innate Immune Cells. *Front Immunol* **12**, 767319 (2021).
15. C. E. Perlman, J. Bhattacharya, Alveolar expansion imaged by optical sectioning microscopy. *J Appl Physiol (1985)* **103**, 1037-1044 (2007).
16. M. N. Islam *et al.*, The mitochondrial calcium uniporter of pulmonary type 2 cells determines severity of acute lung injury. *Nat Commun* **13**, 5837 (2022).
17. Y. Ashino, X. Ying, L. G. Dobbs, J. Bhattacharya, [Ca(2+)](i) oscillations regulate type II cell exocytosis in the pulmonary alveolus. *Am J Physiol Lung Cell Mol Physiol* **279**, L5-13 (2000).
18. J. Gafni *et al.*, Xestospongins: potent membrane permeable blockers of the inositol 1,4,5-trisphosphate receptor. *Neuron* **19**, 723-733 (1997).

19. V. M. Ranieri *et al.*, Effect of mechanical ventilation on inflammatory mediators in patients with acute respiratory distress syndrome: a randomized controlled trial. *Jama* **282**, 54-61 (1999).
20. L. Tremblay, F. Valenza, S. P. Ribeiro, J. Li, A. S. Slutsky, Injurious ventilatory strategies increase cytokines and c-fos m-RNA expression in an isolated rat lung model. *J Clin Invest* **99**, 944-952 (1997).
21. J. A. Frank, C. M. Wray, D. F. McAuley, R. Schwendener, M. A. Matthay, Alveolar macrophages contribute to alveolar barrier dysfunction in ventilator-induced lung injury. *Am J Physiol Lung Cell Mol Physiol* **291**, L1191-1198 (2006).
22. J. Wu *et al.*, Activation of NLRP3 inflammasome in alveolar macrophages contributes to mechanical stretch-induced lung inflammation and injury. *J Immunol* **190**, 3590-3599 (2013).
23. G. A. Gusarova *et al.*, Actin fence therapy with exogenous V12Rac1 protects against acute lung injury. *JCI Insight* **6**, (2021).
24. G. Otulakowski *et al.*, Hypercapnia attenuates ventilator-induced lung injury via a disintegrin and metalloprotease-17. *J Physiol* **592**, 4507-4521 (2014).
25. J. P. Joelsson, S. Ingthorsson, J. Kricker, T. Gudjonsson, S. Karason, Ventilator-induced lung-injury in mouse models: Is there a trap? *Lab Anim Res* **37**, 30 (2021).
26. A. Hidalgo *et al.*, Pulmonary surfactant and drug delivery: Vehiculization, release and targeting of surfactant/tacrolimus formulations. *J Control Release* **329**, 205-222 (2021).

Acknowledgements

This work was supported by an NIH grant HL36024 and DOD grant PR211516 to J.B. L.M. was supported by an AHA Postdoctoral Fellowship (ID: 902655). M.N.I was supported by an American Heart Association (AHA) Grant-in-Aid. Some studies were carried out in the Columbia Center for Translational Immunology Flow Cytometry Core, supported in part by NIH award S10OD020056.

Author Contributions

L.M planned, carried out, analyzed all experiments, and wrote the initial manuscript. G.A.G and M.N.I contributed to imaging experiments. S.B contributed to the plan. J.B. supervised the overall project. L.M and J.B edited the manuscript and all authors approved.

Address for correspondence

Jahar Bhattacharya, Department of Medicine, 630 W. 168th St., Room BB 8-812, New York, New York 10032, USA. Email: jb39@cumc.columbia.edu.

Declaration of interests

The authors declare no competing interests.

Figure Legends

Figure 1. Pseudocolor superimposition by confocal microscopy reveals AM shape protection during lung hyperinflation.

a A single alveolus *(rectangle in i)* was imaged at high power in green *(ii)* and red *(iii)* pseudocolors at the indicated inflation pressures. Image overlay (*iv*) reveals yellow pseudocolor of the merged green and red images at a non-distending segment of the alveolus, but pseudocolor separation at the distending segment (*dashed rectangles*). A sessile AM is located at the corner of the non-distending alveolar segment *(iv). AT1,* alveolar type 1 epithelial cell; *AT2,* alveolar type 2 epithelial cell; *AM,* sessile AM.

b Group data are for AMs (n = 58) counted in 6 fields of view from 6 lungs hyperinflated at alveolar pressure of 15 cmH2O. Scale bars = 10 μm.

c A single AM (star in *i)* imaged at high power shows cell membrane immunofluorescence of SiglecF in green *(ii)* and red *(iii)* pseudocolors for the indicated inflation pressures. AM distension was assessed by pseudocolor superimposition (iii). Bars, mean± SEM. Scale bars = 10 μm.

d Confocal images of AM perimeter (SiglecF staining) at 5 (green) and 15 (red) cmH_2O inflation pressure at different depths. Sketch shows the imaging protocol. The graph plots AM diameter (dashed line) at different depths below the pleura. Replicated 8 times in 8 lungs. Scale bar = 10 μm.

Figure 2. Hyperinflation causes calcium mobilization in sessile AMs.

a Confocal images show Ca^{2+} fluorescence (fluo-4) in a single AM at low (*rectangle in i*) and high (*ii-vi*) power before and after hyperinflation. Pseudocolors represent grey levels per the symbol key.

b Images from adjoining alveoli show AMs that responded with hyperinflation-induced Ca^{2+} increase (AM #3) versus those that did not respond (AMs #1 and #2). Tracings show corresponding time courses. Bars are group data for responders (+) and non-responders (-) as indicated.

c Bars show calcium responses in AMs exposed to buffer alone (*buffer*) or buffer containing xestospongin C (*XeC*). Mean±sem. Numbers of AMs and lungs are indicated.

d Plot shows regression of increase in cytosolic Ca^{2+} in AMs after hyperinflation (*Δ calcium %*) against efficiency of gap junctional communication (*GJC*) quantified in terms of fluorescence recovery after photobleaching (*FRAP %*). Data are for 27 sessile AMs from 4 lungs.

f Bars show % of sessile AMs per field of view that responded to hyperinflation by increasing cCa^{2+} in CD11cCre-Cx43$^{fl/fl}$ mice ($Cx43^{KO}$) and littermate controls ($Cx43^{FL}$). Data show mean±sem. n = 8 ($Cx43^{WT}$) and 5 ($Cx43^{KO}$) lungs per group, 67 ($Cx43^{FL}$) and 62 ($Cx43^{KO}$) AMs per group. Data analyzed by paired t-test except f (non-paired t-test).

Figure 3. Hyperinflation induces TNFa secretion in sessile AMs.

a Confocal image (*i*) shows sessile AMs expressing the indicated fluorescence. Alveolar tracings depict AM distribution (*dotted lines*). Selected AMs (rectangle), imaged at high magnification (*ii, iii*), show TNFα fluorescence after hyperinflation. The tracings quantify the fluorescence.

b Plot shows data for individual AMs from 3 lungs. TNFα secretion is quantified as fluorescence decrease from baseline. *GJC*, gap junction communication; *FRAP %*, fluorescence recovery after photobleaching expressed as difference from initial fluorescence, quantified 60 min after bleaching. Line is drawn by linear regression analysis.
c Confocal images show fluorescence of alveolar epithelium infused with calcein (*i*) and anti-TNFR1 mAb (*ii-iv*) in littermate control mice ($Cx43^{FL}$) and in mice with AM-specific Cx43 knockout ($Cx43^{KO}$) as indicated. Scale bars = 10 um. Bars show the group data. Mean±sem. n = 3 and 4 lungs respectively, for littermate control and KO groups. Data analyzed by unpaired t-test followed by Bonferroni correction for multiple comparisons where necessary.

Figure 4. Sessile AM connexin-43 deletion protects against ventilator-induced lung injury.
Bars show quantifications in the bronchoalveolar lavage **(**BAL) for neutrophil counts (a), protein concentration (b), cytokine and chemokine levels (c) in mice 2 hours after mechanical ventilation at indicated tidal volumes. $Cx43^{FL}$*, littermate control.* $Cx43^{KO}$, CD11cCre-$Cx43^{fl/fl}$. n = 3 ($Cx43^{FL}$), 4 ($Cx43^{KO}$) lungs per group. Data analyzed by unpaired t-test followed by Bonferroni correction for multiple comparisons where necessary.

Figure 5. Liposome encapsulated XeC attenuates ventilator-induced lung injury.
a Confocal images show uptake of FM1-43 labelled surfactant (*i*) in AMs (*ii-iii*) 2 hours after intranasal instillation. Bars are quantification of uptake. Dotted lines trace alveolar perimeters. *FS*, fluorescent surfactant.
b Confocal images show uptake of liposome encapsulated rhodamine b labelled dextran 70 kDa (*i*) in AMs (*ii-iii*) 2 hours after intranasal instillation. Bars are quantification of uptake. Dotted lines trace alveolar perimeters. *FS-lip* fluorescent dextran.
c Bars show calcium responses in AMs in mice intranasally instilled with PBS- or xestospongin C (*XeC*)-encapsulated liposomes 2 hours prior to mechanical ventilation at the indicated tidal volumes. Mean±sem.
d-f Bars show quantifications in the BAL for neutrophil counts (d), protein (e), and the indicated cytokines and chemokines 2 hours after mechanical ventilation at indicated tidal volumes. *XeC*, mice treated with liposomes encapsulating XeC, *PBS*, mice treated with liposomes encapsulating PBS. n = 3 (*PBS*) and 4 (*XeC*) lungs per group. Data for c-f analyzed by unpaired t-test followed by Bonferroni correction for multiple comparisons where necessary.

FIGURE 1

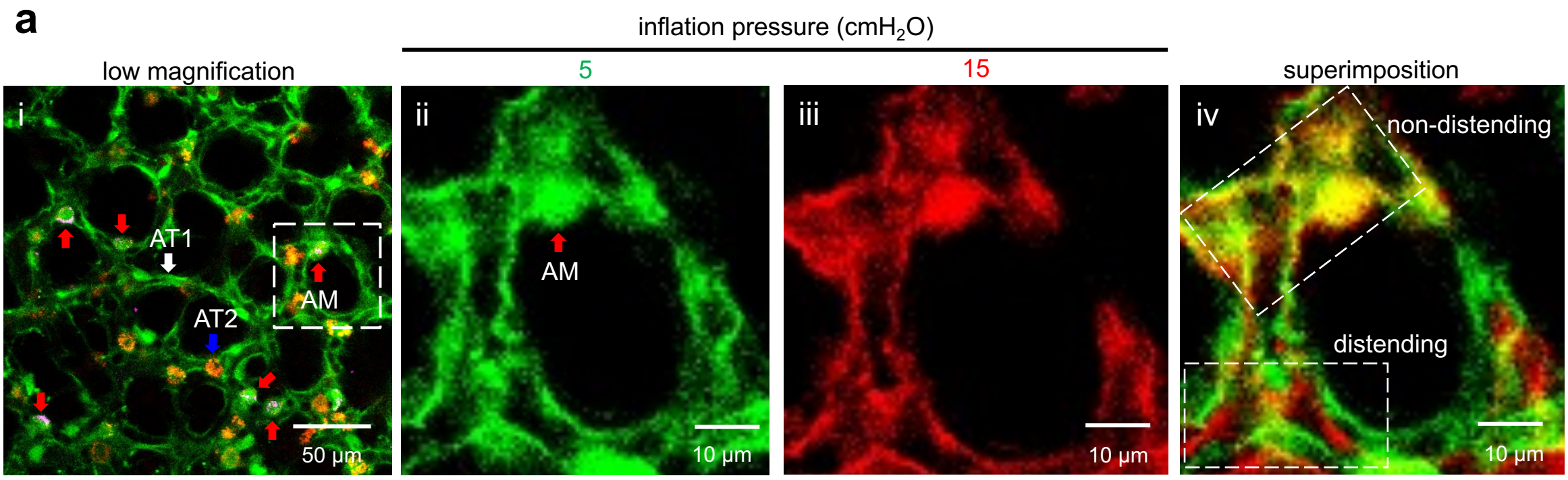
a
inflation pressure (cmH2O)
low magnification
5
15
superimposition
i
ii
iii
iv
AT1
AT2
AM
non-distending
distending
50 µm
10 µm
10 µm
10 µm
Calcein, LTR and SiglecF

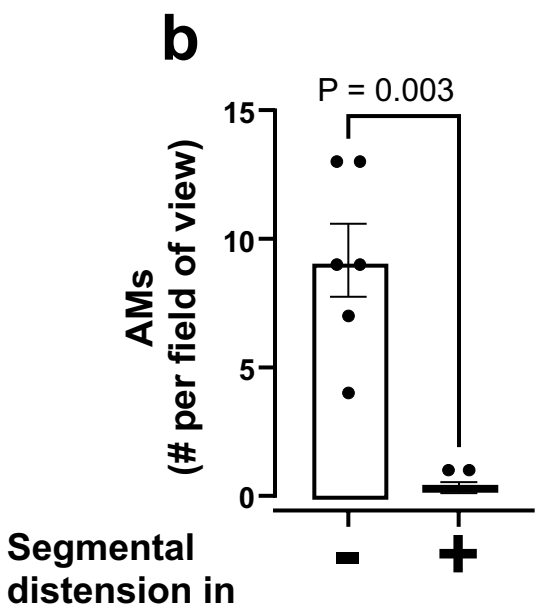
b
P = 0.003
AMs (# per field of view)
15
10
5
0
-
+
Segmental distension in alveolus:

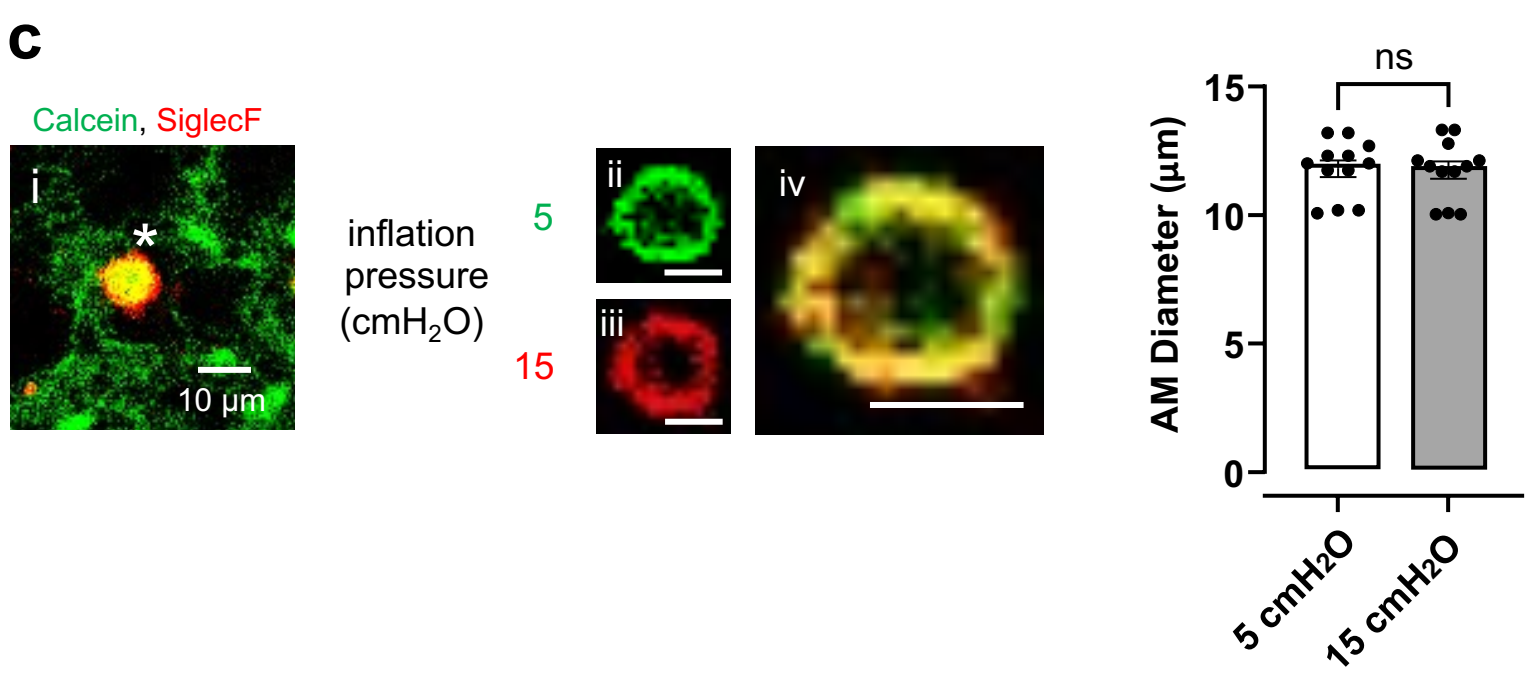
c
Calcein, SiglecF
i
*
10 µm
inflation pressure (cmH2O)
5
15
ii
iii
iv
ns
AM Diameter (µm)
15
10
5
0
5 cmH2O
15 cmH2O

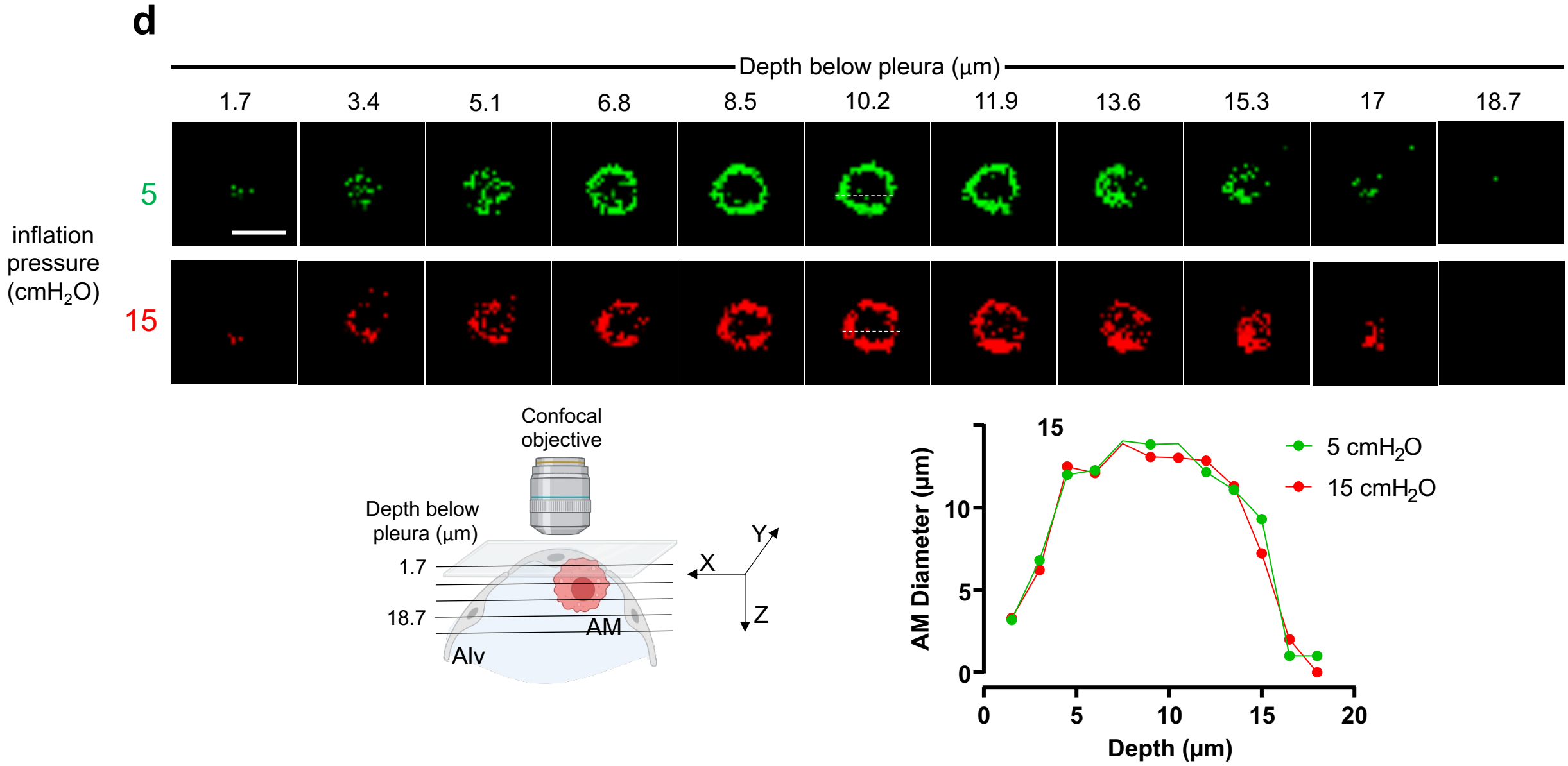
d
Depth below pleura (µm)
1.7
3.4
5.1
6.8
8.5
10.2
11.9
13.6
15.3
17
18.7
inflation pressure (cmH2O)
5
15
Confocal objective
Depth below pleura (µm)
1.7
18.7
AM
Alv
X
Y
Z
AM Diameter (µm)
15
5 cmH2O
15 cmH2O
10
5
0
0
5
10
15
20
Depth (µm)

FIGURE 2

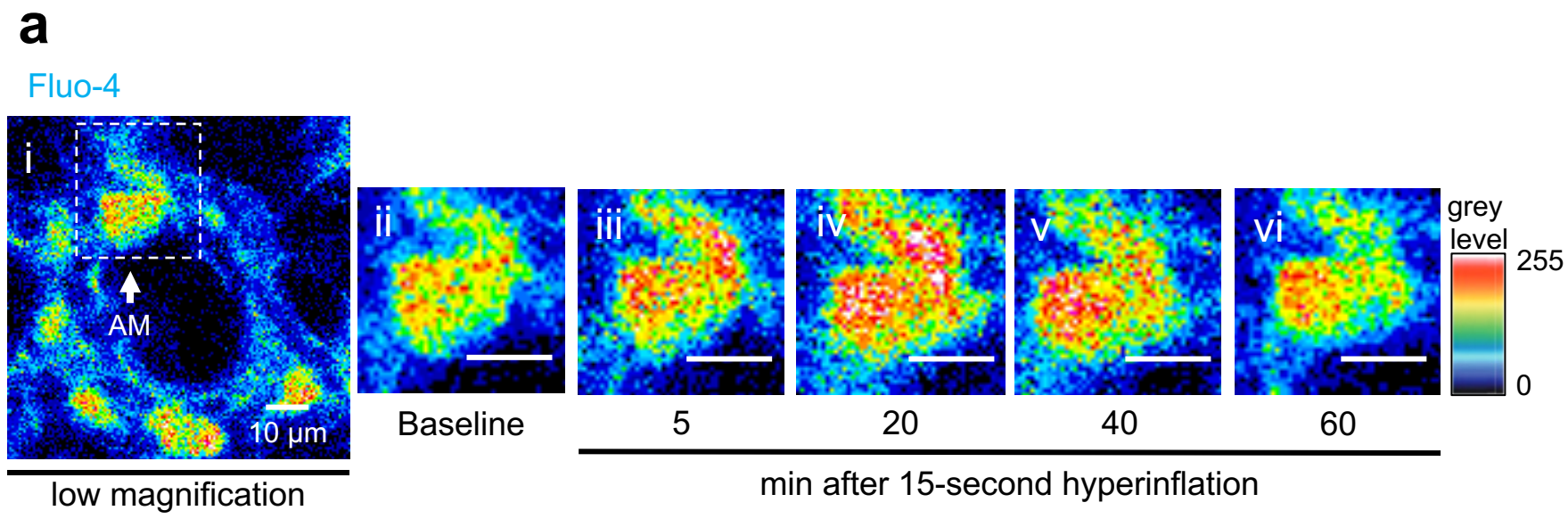
a
Fluo-4
i
AM
10 µm
low magnification
ii
iii
iv
v
vi
Baseline
5
20
40
60
min after 15-second hyperinflation
grey level
255
0

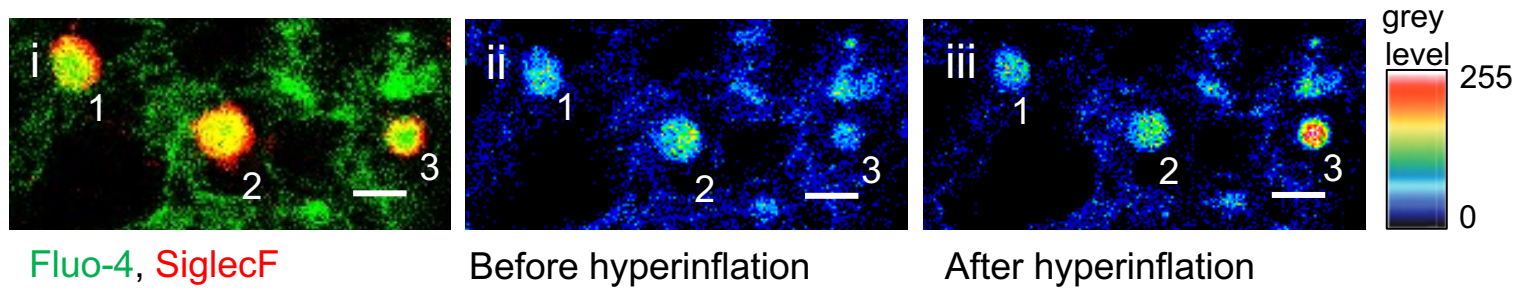
b
i
ii
iii
1
2
3
Fluo-4, SiglecF
Before hyperinflation
After hyperinflation
grey level
255
0

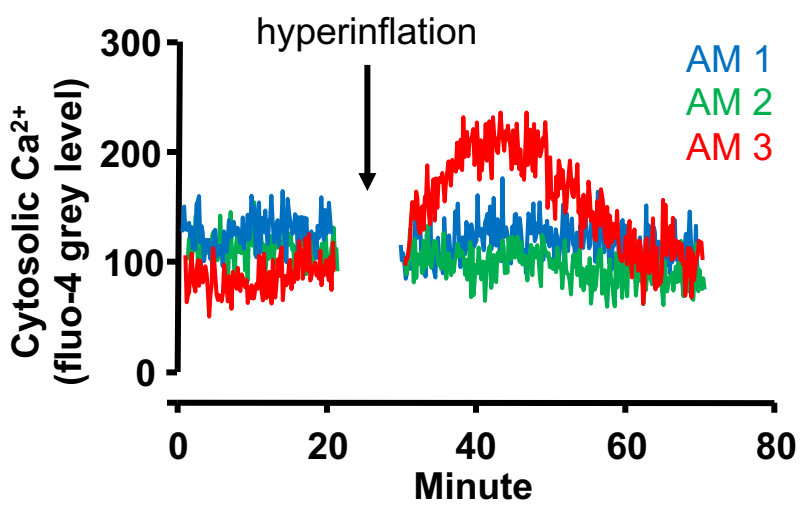
hyperinflation
AM 1
AM 2
AM 3
Cytosolic Ca2+ (fluo-4 grey level)
300
200
100
0
0
20
40
60
80
Minute

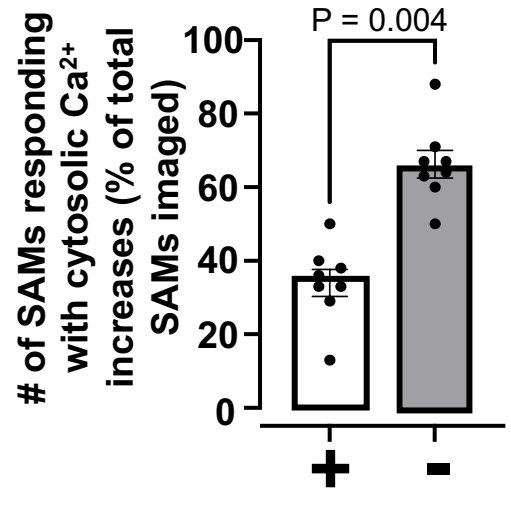
P = 0.004
# of SAMs responding with cytosolic Ca2+ increases (% of total SAMs imaged)
100
80
60
40
20
0
+
-
AMs 22 45

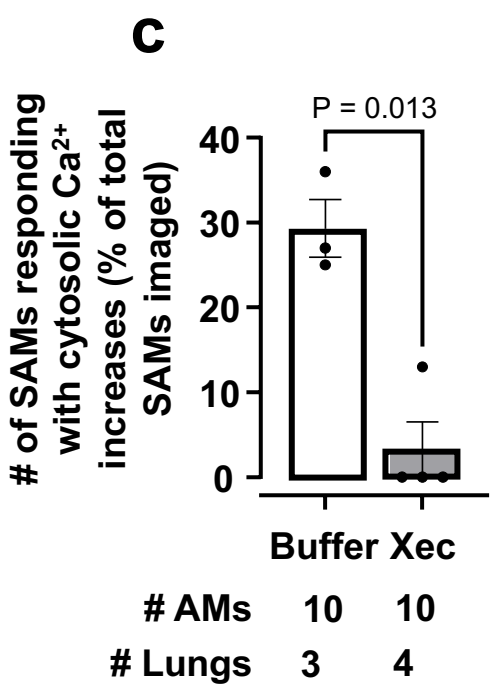
c
P = 0.013
# of SAMs responding with cytosolic Ca2+ increases (% of total SAMs imaged)
40
30
20
10
0
Buffer Xec
AMs 10 10
Lungs 3 4

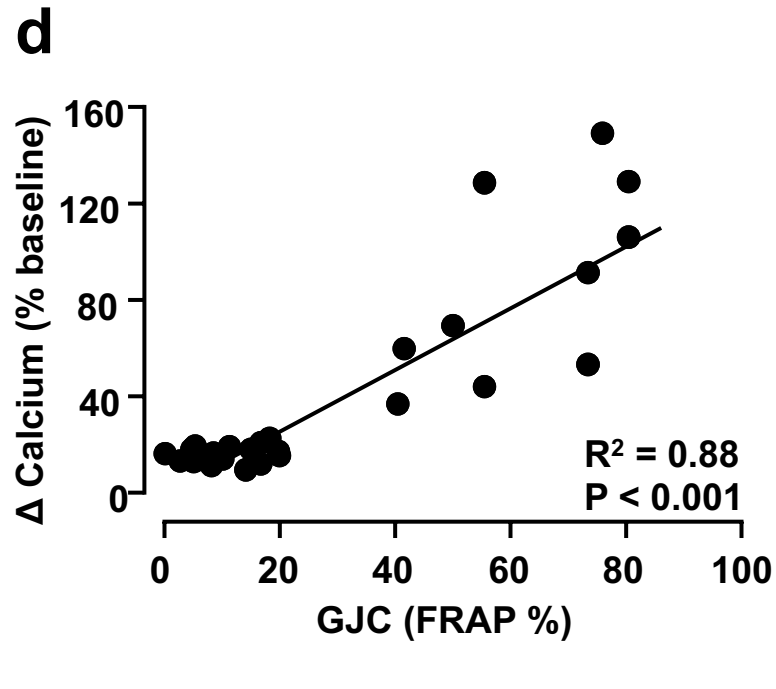
d
Δ Calcium (% baseline)
160
120
80
40
0
R2 = 0.88
P < 0.001
0
20
40
60
80
100
GJC (FRAP %)

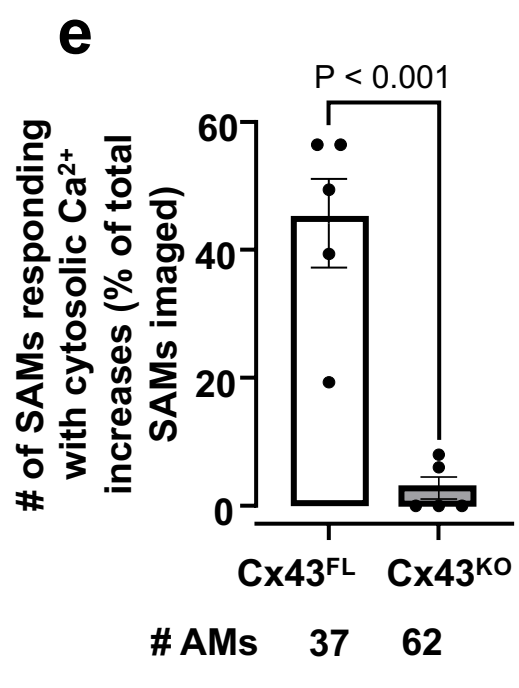
e
P < 0.001
# of SAMs responding with cytosolic Ca2+ increases (% of total SAMs imaged)
60
40
20
0
Cx43FL
Cx43KO
AMs 37 62

FIGURE 3

a

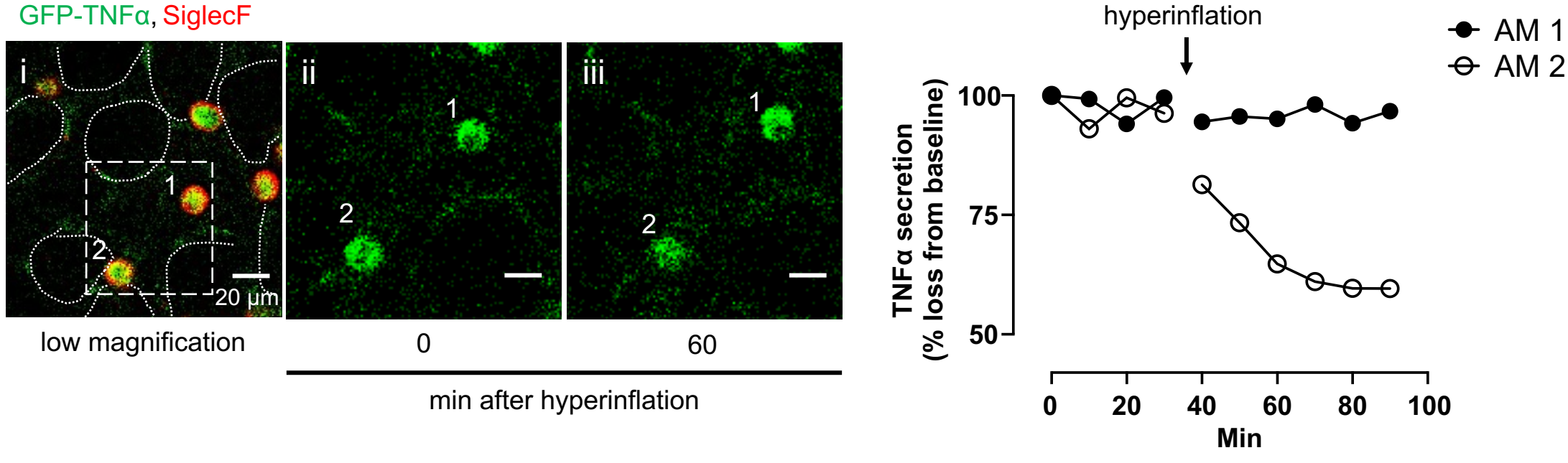
GFP-TNFα, SiglecF
i
ii
iii
1
2
20 μm
low magnification
0
60
min after hyperinflation
hyperinflation
AM 1
AM 2
TNFα secretion
(% loss from baseline)
100
75
50
0
20
40
60
80
100
Min

b

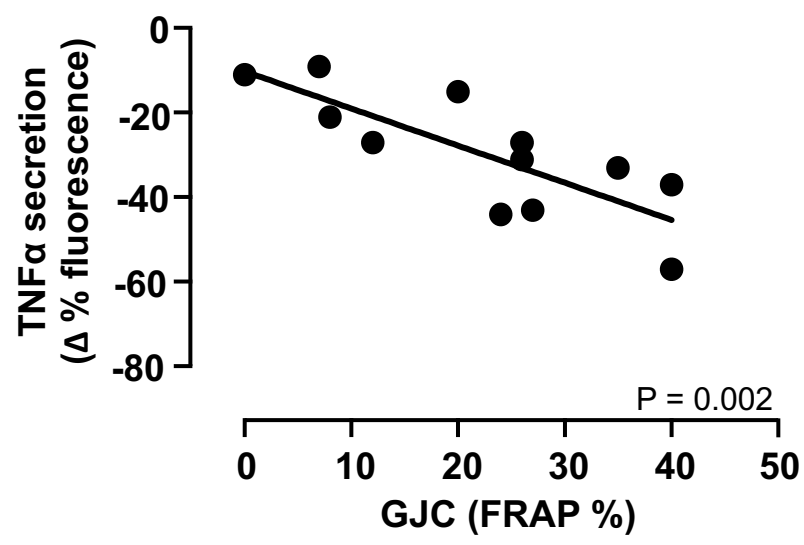
TNFα secretion
(Δ % fluorescence)
0
-20
-40
-60
-80
P = 0.002
0
10
20
30
40
50
GJC (FRAP %)

c

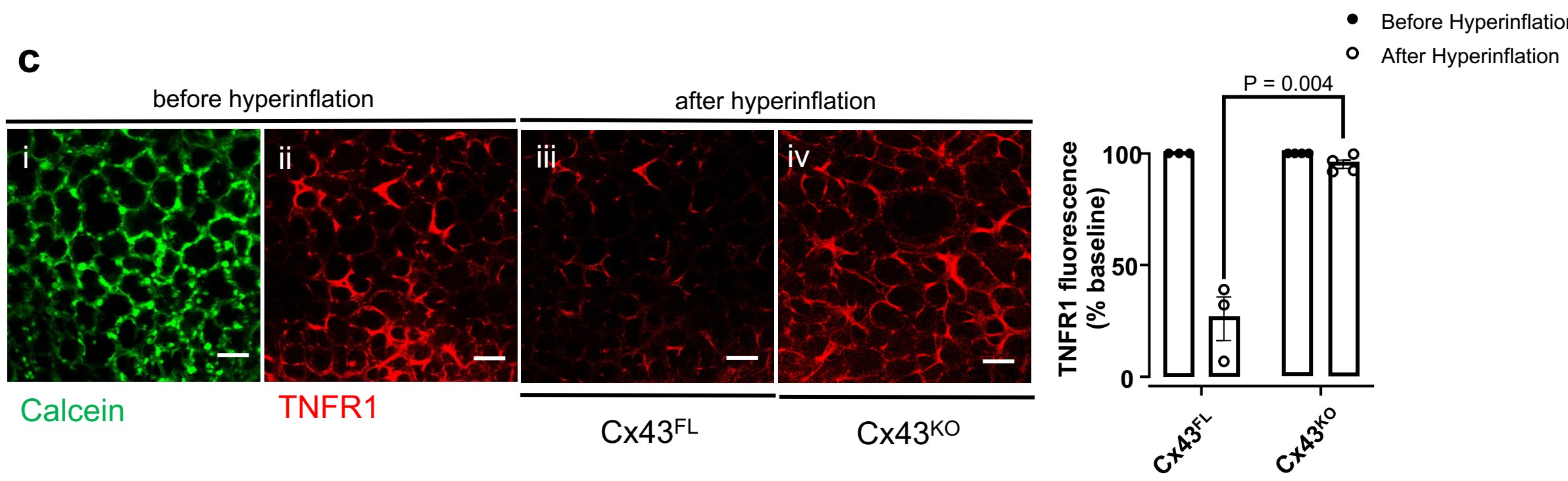
before hyperinflation
after hyperinflation
i
ii
iii
iv
Calcein
TNFR1
Cx43FL
Cx43KO
Before Hyperinflation
After Hyperinflation
P = 0.004
TNFR1 fluorescence
(% baseline)
100
50
0
Cx43FL
Cx43KO

FIGURE 4

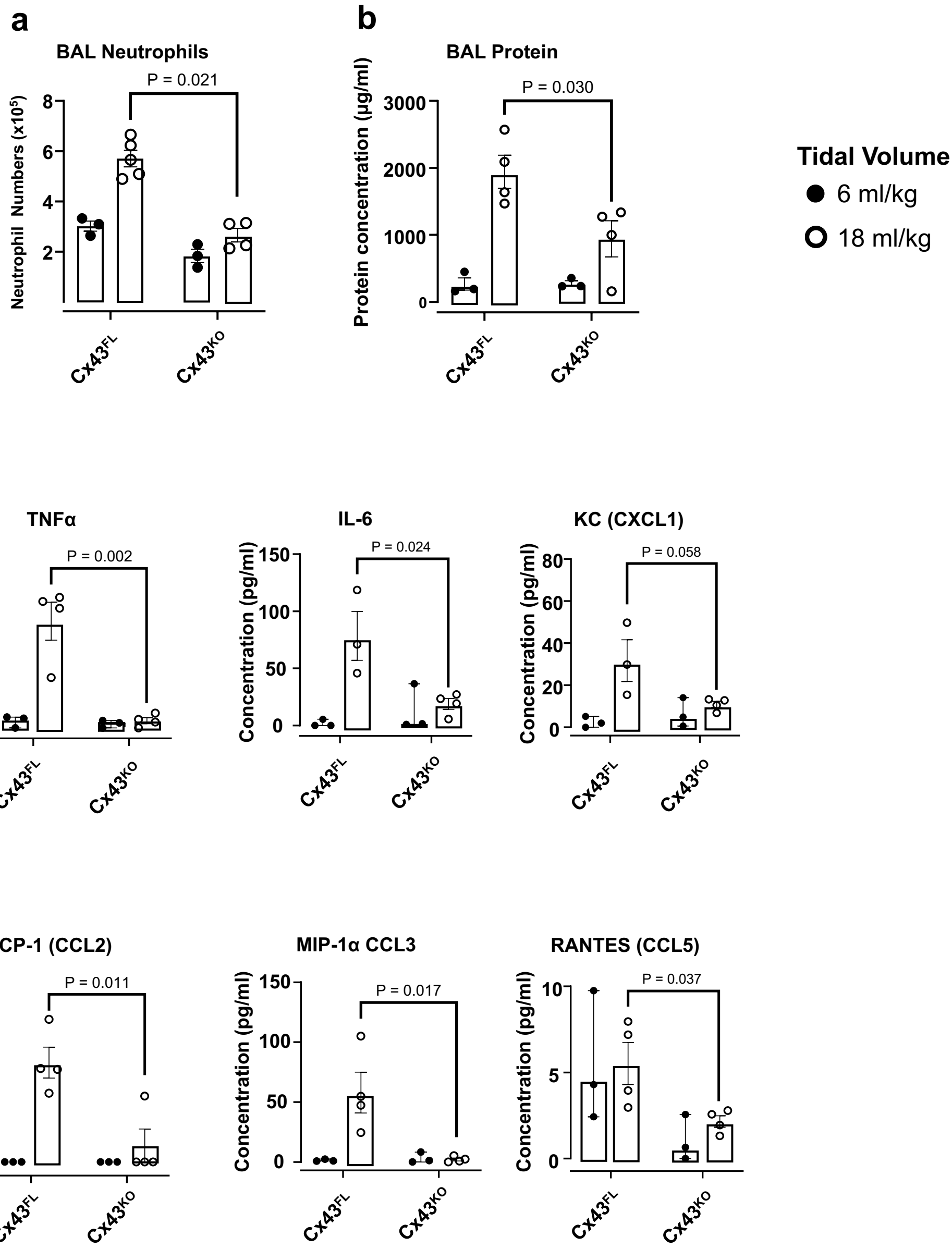
a
BAL Neutrophils
P = 0.021
Neutrophil Numbers (x10⁵)
8
6
4
2
Cx43FL
Cx43KO
b
BAL Protein
P = 0.030
Protein concentration (µg/ml)
3000
2000
1000
0
Cx43FL
Cx43KO
Tidal Volume
6 ml/kg
18 ml/kg
c
TNFα
P = 0.002
Concentration (pg/ml)
20
15
10
5
0
Cx43FL
Cx43KO
IL-6
P = 0.024
Concentration (pg/ml)
150
100
50
0
Cx43FL
Cx43KO
KC (CXCL1)
P = 0.058
Concentration (pg/ml)
80
60
40
20
0
Cx43FL
Cx43KO
MCP-1 (CCL2)
P = 0.011
Concentration (pg/ml)
80
60
40
20
0
Cx43FL
Cx43KO
MIP-1α CCL3
P = 0.017
Concentration (pg/ml)
150
100
50
0
Cx43FL
Cx43KO
RANTES (CCL5)
P = 0.037
Concentration (pg/ml)
10
5
0
Cx43FL
Cx43KO

FIGURE 5

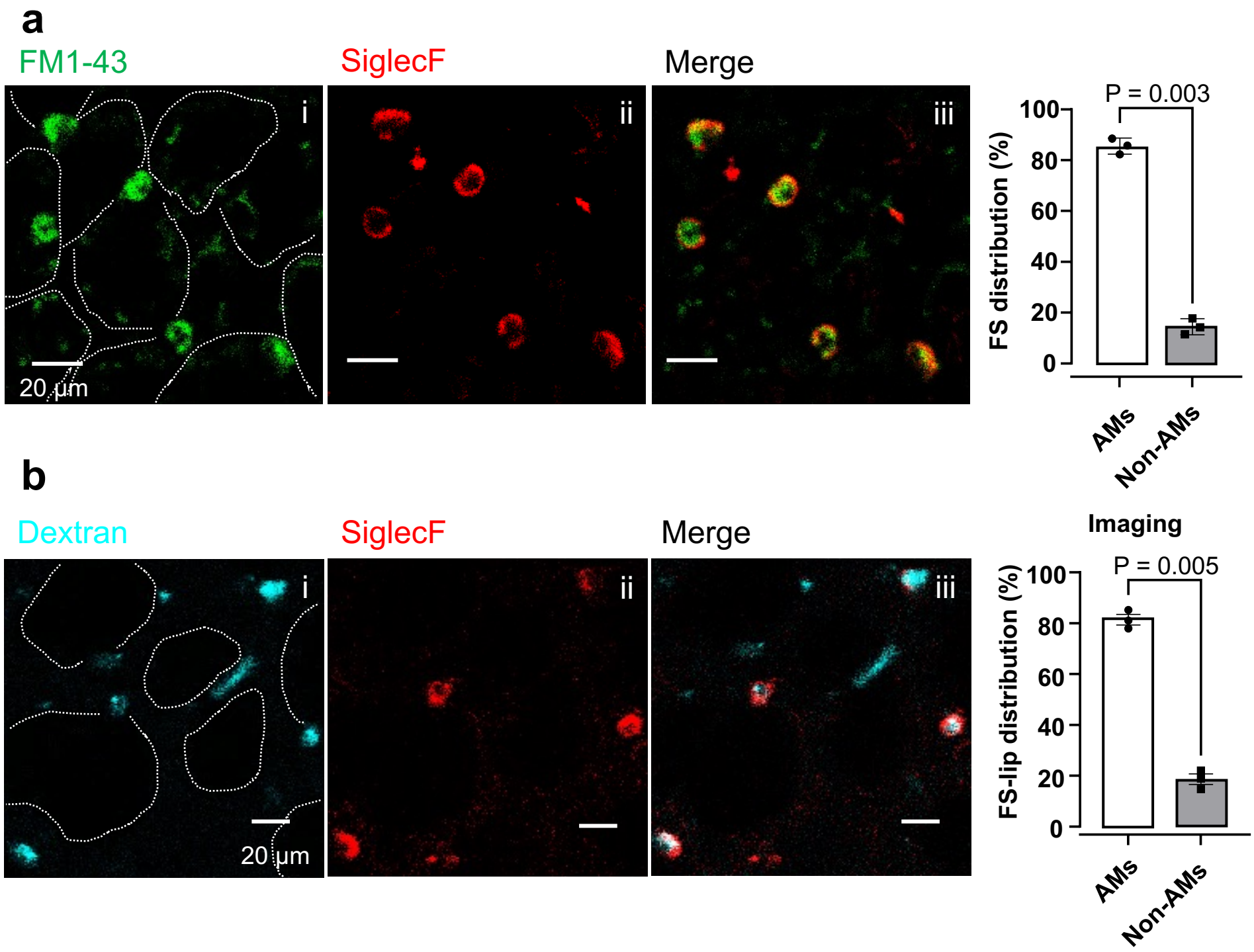
a
FM1-43
SiglecF
Merge
i
ii
iii
20 µm
P = 0.003
FS distribution (%)
100
80
60
40
20
0
AMs
Non-AMs
b
Dextran
SiglecF
Merge
i
ii
iii
20 µm
Imaging
P = 0.005
FS-lip distribution (%)
100
80
60
40
20
0
AMs
Non-AMs
c
P = 0.001
# of SAMs responding with cytosolic Ca2+ increases (% of total SAMs imaged)
60
40
20
0
PBS
XeC
d
BAL Neutrophils
P = 0.011
Neutrophil Numbers (x10^5)
10
8
6
4
2
PBS
XeC
e
BAL Protein
P = 0.034
BAL Protein (µg/ml)
4000
3000
2000
1000
0
PBS
XeC
Tidal Volume
6 ml/kg
18 ml/kg
f
TNFα
P = 0.004
Concentration (pg/ml)
150
100
50
0
PBS
XeC
IL-6
P = 0.024
Concentration (pg/ml)
5000
4000
3000
2000
1000
0
PBS
XeC
KC (CXCL1)
P = 0.022
Concentration (pg/ml)
1000
800
600
400
200
0
PBS
XeC
MCP-1 (CCL2)
P < 0.001
Concentration (pg/ml)
250
200
150
100
50
0
PBS
XeC
MIP-1α (CCL13)
P = 0.071
Concentration (pg/ml)
500
400
300
200
100
0
PBS
XeC
RANTES (CCL5)
P = 0.004
Concentration (pg/ml)
25
20
15
10
5
0
PBS
XeC

Supplementary material to:

Sessile alveolar macrophage connexin-43 determines mechano-immunity in the lung

Liberty Mthunzi[1], Galina A Gusarova[1], Mohammad N Islam[1], Sunita Bhattacharya[1], Jahar Bhattacharya[1]

[1]Lung Biology Laboratory, Division of Pulmonary Allergy and Critical Care, Department of Medicine, Vagelos College of Physicians and Surgeons, Columbia University, New York, NY 10032

*Correspondence to: jb39@cumc.columbia.edu

Materials and Methods

Materials. A list of antibodies used in this study is available in the supplementary material (**sTable 1**). We purchased mAb MCA2350 against the TNFR1 extracellular epitope (40 μg/ml) from AbD Serotec (Oxford, UK). Anti-TNFR1 antibody was fluorescently labeled with Alexa Fluor 633 using standard protocols. Fluo-4 AM (5 μM), Lysotracker Red (LTR, 100 nM), calcein AM (5 μM), FM1-43 (5 μM) and rhodamine-B labelled dextran 70 kDa (80 μg), were purchased from Thermo-Fisher Scientific (Waltham, MA). Xestospongin C (XeC, 20 μM) was purchased from Sigma-Aldrich (St. Louis, MO). We purchased human recombinant TNFα (10 ng/ml) from BD Biosciences (San Jose, CA). We purchased lung surfactant (CUROSURF®, poractant alfa) from Chiesi Farmaceutici (Parma, Italy) and it was used at a final concentration of 5 mg/ml. Vehicle for fluorophores, antibodies and other agents was HEPES buffer (see below for composition).

Mouse care. All mouse procedures were reviewed and approved by the institutional animal care and use committee (IACUC) at Columbia University Irving Medical Center. All mice were cared for according to the National Institutes of Health (NIH) guidelines for the care and use of laboratory animals. Mice were socially housed under a 12 h light/dark cycle with *ad libitum* access to water and food. The mice were inbred hence no randomization was required. Nevertheless, we randomly assigned male and female age-matched mice to experimental groups. Mice were between 2–4 months and on a C57BL/6J background. *CD11cCre*$^{+/-}$ mice were provided by Boris Reizis while *Cx43*$^{flox/flox}$ (stock no. 008039) and C57BL/6J (stock no. 000664) mice were purchased from the Jackson Laboratory and bred in house.

Isolated and perfused lung preparation. Using our reported methods (*1-5*), we excised lungs from anesthetized (I.P., ketamine 100 mg/kg, xylazine 10 mg/kg) and heparinized (1000 IU/kg) mice then perfused them with autologous blood through cannulas in the pulmonary artery and left atrium (**sFig. 1**). We diluted the blood in HEPES buffer (150 mmol/l Na^+, 5 mmol/l K^+, 1.0 mmol/l Ca^{2+}, 1 mmol/l Mg^{2+}, and 20 mmol/l HEPES, pH 7.4) containing 4% (w/v) dextran (70 kDa) and 1% FBS to a final hematocrit of 20%. The HEPES buffer had an osmolarity of 300 mosM (Fiske Micro-Osmometer, Fiske® Associates, Norwood, MA). We set the perfusion flow rate to 0.5 ml/min at 37°C. Lungs were inflated with room air through a tracheal cannula. We held the pulmonary artery, left atrial and airway pressures at 10, 3 and 5 cmH_2O respectively during microscopy.

Alveolar micropuncture and microinfusion. To load the alveoli with fluorescent dyes, microspheres, and antibodies, we micropunctured single alveoli with glass micropipettes (tip diameter of 7 μm) and ~7 neighboring alveoli were microinfused (**sFig. 1**) (*6*). For each bolus, the micropunctured alveolus was microinfused for ~3 s, to instill ~0.5 nl solution. After each microinfusion, the free liquid in the alveolar lumen drained in seconds re-establishing air-filled alveoli (*6*). This rapid clearance indicates that the micropuncture did not rupture the alveolar wall, and that the micropunctured membrane rapidly resealed as reported for other cells (*7*). Nevertheless, we selected non-micropunctured alveoli for imaging. To determine whether the fluorescence detected in the epithelium was intracellular or extracellular, in some experiments we microinfused alveoli with trypan blue (0.01% w/v, Thermofisher, Waltham, MA), which eliminates extracellular fluorescence (*8*). In all experiments in which multiple dyes were infused, we confirmed absence of bleed-through between fluorescence emission channels.

In vivo lung transfection. GFP-TNFα plasmid (plasmid #28089) was purchased from Addgene (Watertown, MA). Using our established methods (*1*), we complexed plasmid DNA (80 μg) with freshly extruded liposomes (20 μg/μl; 100 nm pore size; DOTAP, Avanti Lipids) in sterile Opti-MEM (Invitrogen, Carlsbad, CA). We administered a plasmid DNA–liposome mix by intranasal instillation (I.N.) of anesthetized mice. Imaging experiments were carried out 48 hours after transfection.

Imaging. We imaged intact alveoli in a 1.7-μm-thick optical section (512 x 512 pixels) at a focal plane ~20 μm deep to the pleural surface of live lungs with laser scanning microscopy (TCS SP8, Leica Microsystems, Wetzlar, Germany) using a x10 air objective (numerical aperture 0.3, Leica Microsystems, Wetzlar, Germany) or ×25 water immersion objective (numerical aperture 0.95, Leica Microsystems, Wetzlar, Germany). For Z stacks, we imaged 1.7-μm-thick optical sections (512 x 512 pixels) at vertical intervals of 1.7 μm from the pleural surface to a depth of 40 μm. To immerse the x25 objective in water, we placed a water drop on a coverslip that was held in a metal O-ring, as described previously (*1, 2, 4, 5*). We used our reported methods to detect fluorescence of microinfused dyes and antibodies in live alveoli (*1, 2, 4, 5*). Cytosolic Ca^{2+} (cCa^{2+}) was detected using fluo-4 as previously reported (*5*). We recorded cCa^{2+} responses at one image/10 s. All images were recorded as single images and processed using MetaMorph imaging software (v7.8, Molecular Devices) or Image J (v15.3, National Institutes of Health). We applied brightness and contrast adjustments to individual pseudocolor channels of entire images and equally to all experimental groups. No further downstream processing or averaging was applied.

Lung hyperinflation. To induce lung hyperinflation, we increased airway pressure from 5 to 15 cmH_2O for 15 seconds. We identified the pre-hyperinflation optical section using morphological landmarks as previously described (*9*). To confirm alveolar stretch due to hyperinflation, we recorded the time dependent secretion of surfactant by alveolar type II cells as loss of lysotracker red (LTR) fluorescence post hyperinflation as previously described (*10*) (**sFig. 2a-c**).

Intranasal instillation. For intranasal instillation, mice were anaesthetized then instilled (2 ml/kg) volume of instillate and allowed to recover for 2 hours prior to experiment.

Mechanical ventilation. A previously described mechanical ventilation (MV) protocol with modifications was used (*11*). Briefly, mice were anesthetized with isoflurane (4%) and ketamine (50 mg/kg) and xylazine (5 mg/kg) administered I.P. A tracheal cannula (PE-90 tubing, BD, Franklin Lakes, NJ) was inserted and secured into place by suture, and MV was started with a tidal volume of 6 ml/kg, a positive end-expiratory pressure (PEEP) of 5 cmH_2O and a respiratory rate of 120 breaths/min (VentElite, Harvard Apparatus, Holliston, MA). Following a 10-min stable baseline period, in some experiments tidal volume was incrementally increased to 18 ml/kg over 5 minutes for high tidal volume ventilation. Depth of anesthesia was assessed by reaction to paw pinch throughout the protocol. Anesthesia was maintained with ketamine (20 mg/kg) and xylazine (2 mg/kg) both administered by I.P injection. MV was continued for 2 hours. Saline (2 ml/kg) was administered by I.P injection throughout the protocol. Blood oxygen saturation, airway pressures, blood pressure, temperature and heart rate were monitored continuously using a computer-integrated data collection system (MouseOx Plus, Starr Life Sciences, Oakmont, PA). Temperature was monitored using a rectal probe and temperature was maintained at 37 °C throughout the protocol using a heating blanket (Homeothermic Blanket

Control Unit, Harvard Apparatus, Holliston, MA). After 2 hours of MV, BAL was performed for analysis of BAL fluid and ALI was evaluated.

Analysis of BAL fluid. The lungs of mice were lavaged repeatedly (5x) with the same 1 ml ice-cold PBS (Ca^{2+} and Mg^{2+} free) through a tracheal cannula. Collected BAL fluid was centrifuged for 4 minutes at 400 g at 4°C. The supernatant was analyzed for protein and cytokine concentrations. We measured TNFα, IL-6, KC (CXCL-1), MCP-1 (CCL2), MCP-1α (CCL3) and RANTES (CCL5) concentrations in BAL fluid to determine pro-inflammatory cytokine secretion. Sample testing was carried out by Quansys Biosciences using a multiplex chemiluminescence assay (Q-plex) for the detection of mouse cytokines and chemokines.

Evaluation of ALI. We evaluated ALI by assessing BAL protein content by BCA assay (Thermo Fisher, Waltham, MA) to determine protein leak from vascular compartment into alveoli. We also assessed ALI by characterizing cell populations in BAL by flow cytometry.

Flow cytometry analysis of BAL cells. Briefly, BAL cell pellet was resuspended in PBS (Ca^{2+} and Mg^{2+} free) supplemented with 1% FBS, 100 mM HEPES. and used for flow cytometry studies. Relevant antibodies were added to the cell suspension and incubated away from direct light for 1 hour at room temperature. The cells were centrifuged (4 min, 4 °C, 400 g) and resuspended in buffer. This procedure was repeated two more times and the cells were finally resuspended in 300 ul PBS (Ca^{2+} and Mg^{2+} free) without supplements. We analyzed cells by flow cytometry (3L Cytek Aurora, Becton Dickinson, NJ) according to manufacturer's protocols using standard software (FCS Express 7 Flow, De Novo Software). Neutrophils were identified as CD45+Ly6G+CD11b+ cells following a standard protocol (**sFig. 6a**) (*12*).

Flow cytometry analysis of liposome uptake by lung cells. Mice were I.N. instilled with 80 µg rhodamine-B labelled dextran 70 kDa (Thermo Fisher, Waltham, MA) complexed in liposomes suspended in a surfactant-PBS (Ca^{2+} and Mg^{2+} free) suspension (5 mg/ml). 60 µl of liposome-surfactant suspension was instilled. 2 hours later, we isolated lung cells. To isolate cells, we buffer (PBS, Ca^{2+} and Mg^{2+} free) perfused lungs through vascular cannulas to clear blood; we then minced and passed the tissue through 40 µm cell strainers (BD Biosciences) to obtain a single cell suspension. For flow cytometry, we surface stained the cells by incubating the suspension with relevant antibodies away from direct light for 1 hour at room temperature. We analyzed cells by flow cytometry (5L Cytek Aurora, Becton Dickinson, NJ) according to manufacturer's protocols using standard software (FCS Express 7 Flow, De Novo Software). Alveolar macrophages were identified as CD45+SiglecF+CD11c+ cells following a standard protocol (**sFig. 6a**) (*12*).

Statistics*.* All groups comprised a minimum of 3 mice each. Group numbers were designed to enable detection of statistically significant differences with a power of at least 85%. For applicable imaging experiments, we carried out a paired protocol, where baseline and test conditions were obtained in the same alveolus or cell, and at least 8 determinations were obtained per lung. These determinations were averaged to obtain a mean for each condition in each lung. There was no statistically significant within-lung variability of effect size. The means for each lung were pooled for the group to obtain mean±sem, where *n* represents the number of lungs unless otherwise stated. The per lung means are shown in the bar diagrams unless otherwise stated. Data are shown as mean±sem. We analyzed paired data by the paired t-test and non-paired data by unpaired t-test. Bonferroni correction was applied for multiple comparisons where necessary. Significance was accepted at $P < 0.05$.

References

1. G. A. Gusarova *et al.*, Actin fence therapy with exogenous V12Rac1 protects against acute lung injury. *JCI Insight* **6**, (2021).
2. J. L. Hook *et al.*, Disruption of staphylococcal aggregation protects against lethal lung injury. *J Clin Invest* **128**, 1074-1086 (2018).
3. R. F. Hough *et al.*, Endothelial mitochondria determine rapid barrier failure in chemical lung injury. *JCI Insight* **4**, (2019).
4. M. N. Islam, G. A. Gusarova, E. Monma, S. R. Das, J. Bhattacharya, F-actin scaffold stabilizes lamellar bodies during surfactant secretion. *Am J Physiol Lung Cell Mol Physiol* **306**, L50-57 (2014).
5. K. Westphalen *et al.*, Sessile alveolar macrophages communicate with alveolar epithelium to modulate immunity. *Nature* **506**, 503-506 (2014).
6. P. M. Wang, Y. Ashino, H. Ichimura, J. Bhattacharya, Rapid alveolar liquid removal by a novel convective mechanism. *Am J Physiol Lung Cell Mol Physiol* **281**, L1327-1334 (2001).
7. R. A. Steinhardt, G. Bi, J. M. Alderton, Cell membrane resealing by a vesicular mechanism similar to neurotransmitter release. *Science* **263**, 390-393 (1994).
8. D. J. Rowlands *et al.*, Activation of TNFR1 ectodomain shedding by mitochondrial Ca2+ determines the severity of inflammation in mouse lung microvessels. *J Clin Invest* **121**, 1986-1999 (2011).
9. C. E. Perlman, J. Bhattacharya, Alveolar expansion imaged by optical sectioning microscopy. *J Appl Physiol (1985)* **103**, 1037-1044 (2007).
10. Y. Ashino, X. Ying, L. G. Dobbs, J. Bhattacharya, [Ca(2+)](i) oscillations regulate type II cell exocytosis in the pulmonary alveolus. *Am J Physiol Lung Cell Mol Physiol* **279**, L5-13 (2000).
11. J. A. Frank, C. M. Wray, D. F. McAuley, R. Schwendener, M. A. Matthay, Alveolar macrophages contribute to alveolar barrier dysfunction in ventilator-induced lung injury. *Am J Physiol Lung Cell Mol Physiol* **291**, L1191-1198 (2006).
12. A. V. Misharin, L. Morales-Nebreda, G. M. Mutlu, G. R. Budinger, H. Perlman, Flow cytometric analysis of macrophages and dendritic cell subsets in the mouse lung. *Am J Respir Cell Mol Biol* **49**, 503-510 (2013).

Supplementary Figure Legends

Supplementary Figure 1. Schematic of isolated, perfused lung preparation and alveolar micropuncture technique.
Lungs are inflated with room air through a cannula in the trachea at a constant inflation pressure of 5 cmH_2O during imaging. Heart and lungs are perfused with autologous blood through cannulae in the pulmonary artery (*PA*) and left atrium (*LA*) at 10 and 3 cmH_2O respectively. Small glass micropipettes are used to microinfuse fluorescent agents into live alveoli.

Supplementary Figure 2. Hyperinflation-induced secretion of surfactant.
a Confocal images show epithelial fluorescence in alveolar epithelium infused with calcein, lysotracker red (LTR) and the anti-siglecF antibody (*i*). Confocal images (*ii-iii*) show LTR fluorescence before and 60 min after hyperinflation.
b Tracings show LTR fluorescence 25 min before and 60 min after hyperinflation.
c Bars show quantifications of LTR fluorescence before and 60 min after hyperinflation. Mean±sem, n = 4 lungs, 49 alveolar epithelial type 2 cells**.**

Supplementary Figure 3. Hyperinflation-induced increases in cCa^{2+} oscillations in AE.
Tracing shows alveolar epithelium cytosolic calcium responses before and after hyperinflation. Note black line, which indicates mean cytosolic calcium. Bars show quantifications of AE cytosolic calcium oscillation amplitude in AE before and after hyperinflation. Mean±sem, n = 3 lungs per group.

Supplementary Figure 4. Sessile AM Cx43 deletion inhibits gap junctional communication.
Confocal image (*i*) shows single a sessile AM in an alveolus. Pseudocolor high power images of sessile AM in (*i*) pre bleach, 0 and 60 min after bleach and post calcein reloading (*ii-v*). White dashed circles indicate photobleached region. Bars show group data quantification of calcein fluorescence within sessile AMs at indicated time points. Mean±sem, n = 4 lungs, 26 sessile AMs.

Supplementary Figure 5. GFP-TNFα fluorescence in sessile AMs.
Confocal image shows TNFα fluorescence was well expressed in imaged sessile AMs. White dashed lines indicate alveolar perimeters. Mean±sem, n = 3 lungs, 20 AMs. *AM*, sessile AM.

Supplementary Figure 6. Flow cytometry gating strategy and liposome uptake.
a Gating strategy used to identify sessile AMs and neutrophils from mouse bronchoalveolar fluid (BAL). A similar strategy was used to identify cells from mouse lung tissue. Cells were isolated from BAL and after the exclusion of debris and doublets, leukocytes were identified by CD45 staining. A sequential gating strategy was used to identify sessile AMs by expression of CD11c and SiglecF and neutrophils by expression of CD11b and Ly6G.
b Bars show distribution of fluorescent liposomes (*FS-lip*) in lung tissue homogenate. Mean±sem, n = 3 lungs. *AM*, sessile AM.

Supplementary Table 1. Table of antibodies used in imaging and flow cytometry studies.
Final conc. indicates concentration used in experiments.

SUPPLEMENTARY FIGURE 1

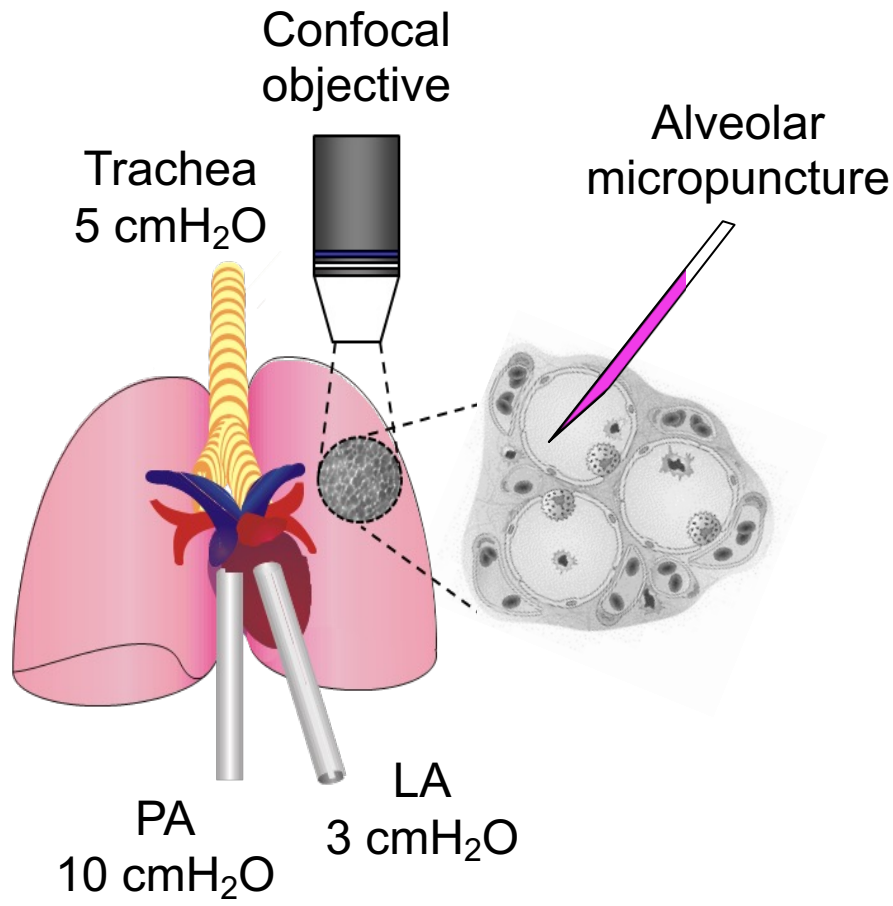

SUPPLEMENTARY FIGURE 2

a

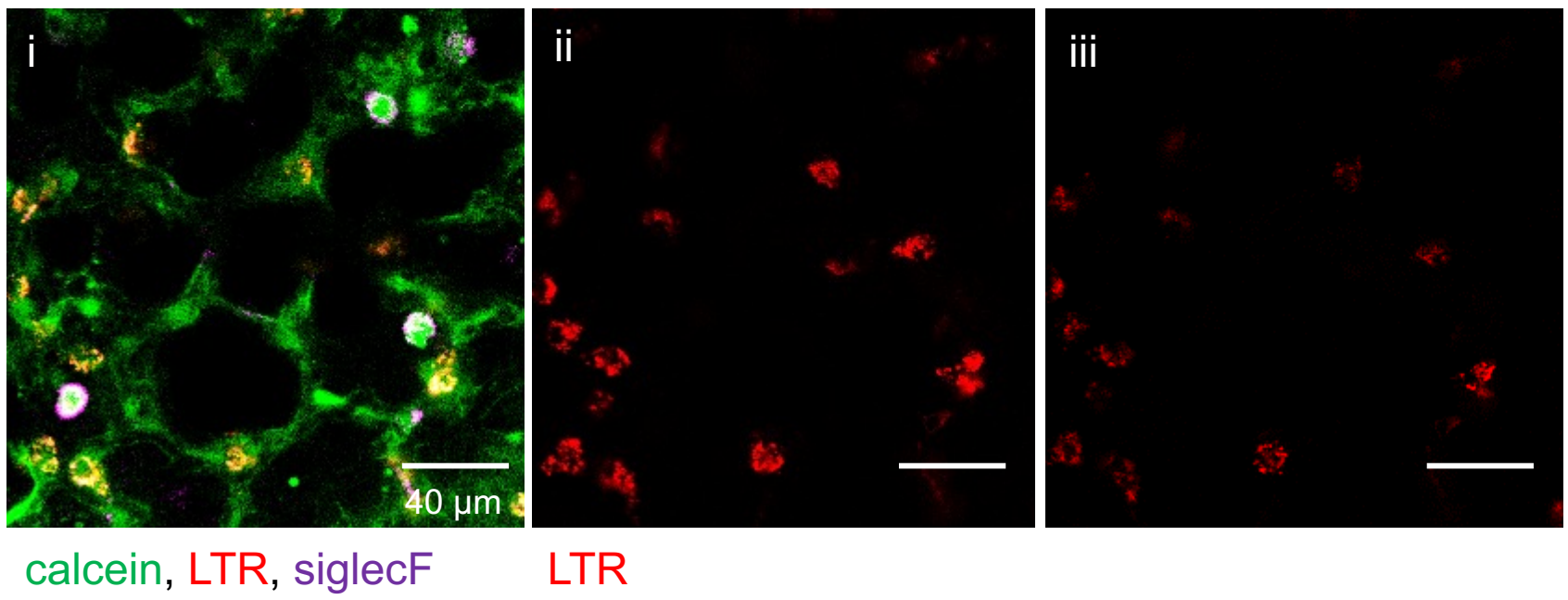

b

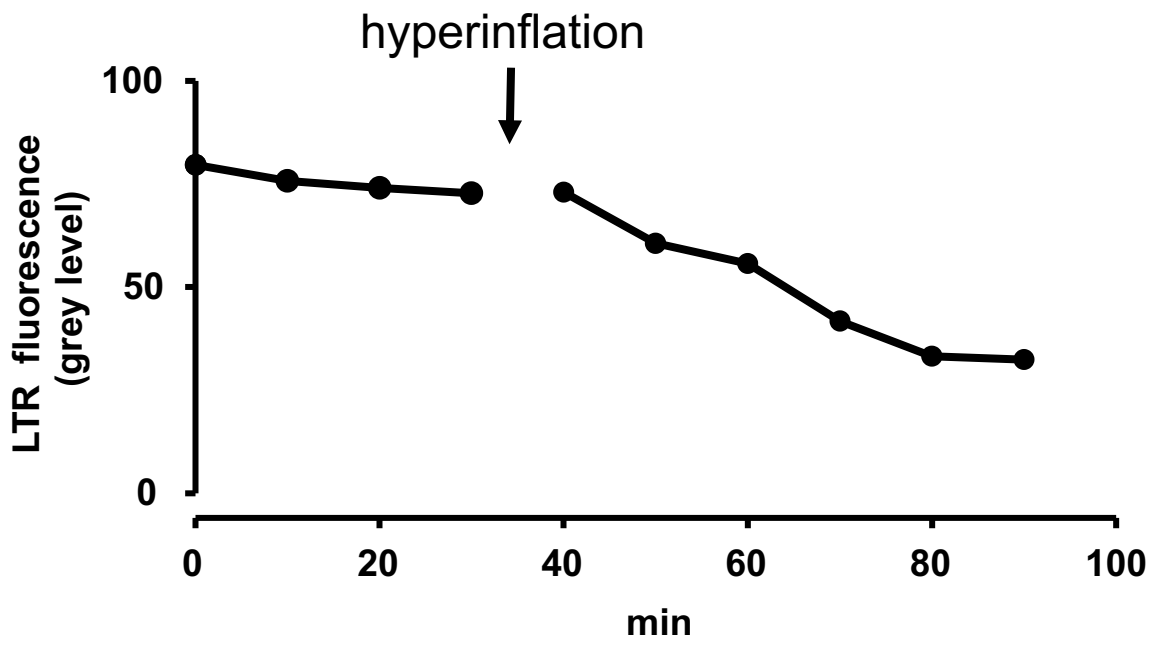

c

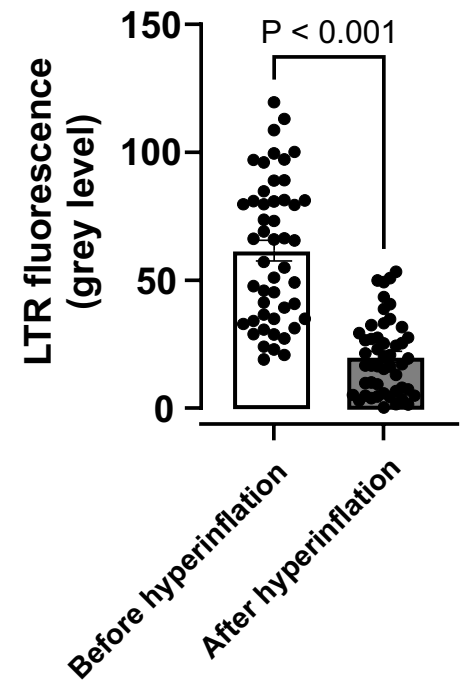

SUPPLEMENTARY FIGURE 3

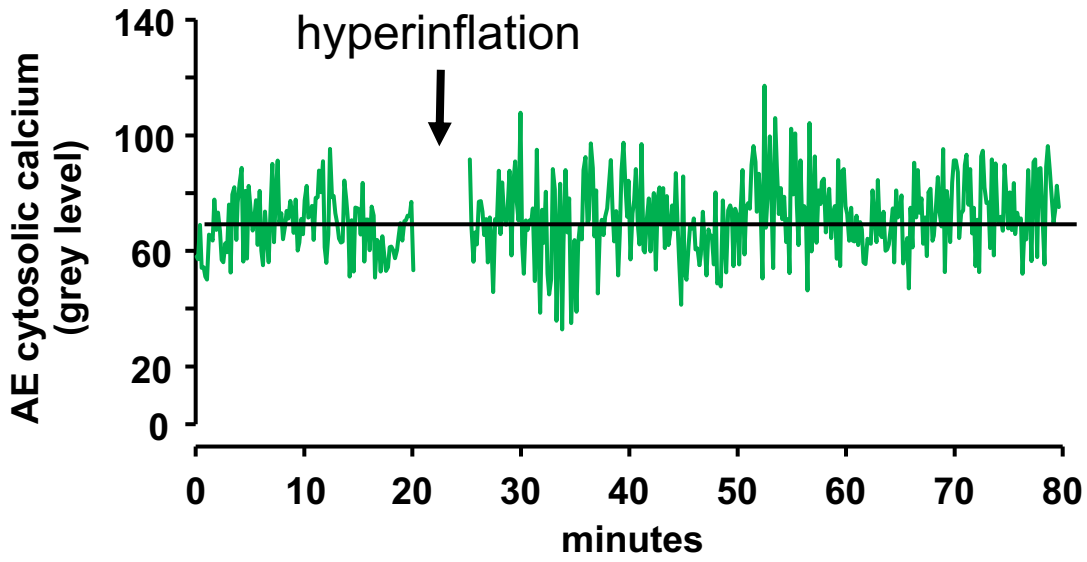

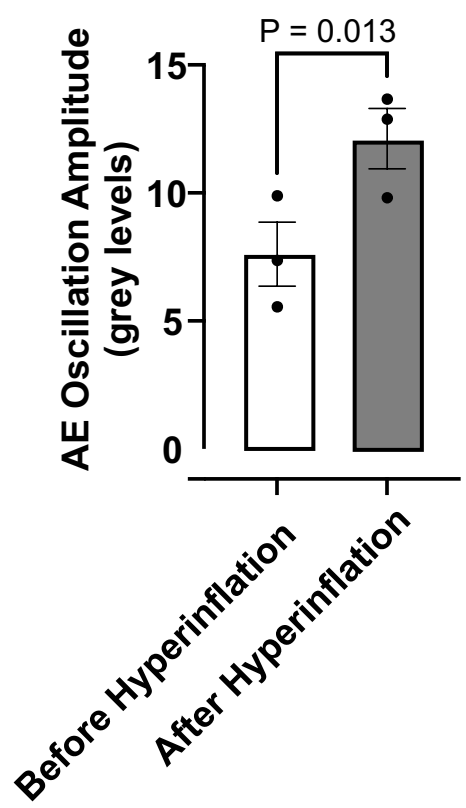

SUPPLEMENTARY FIGURE 4

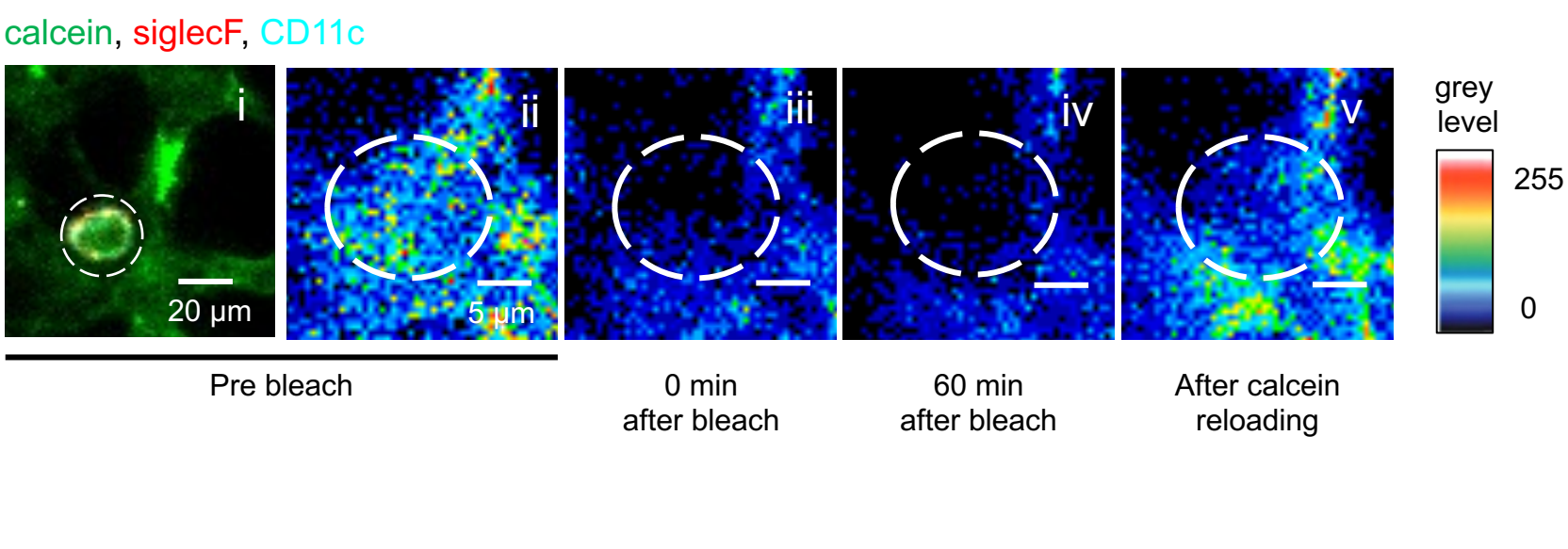

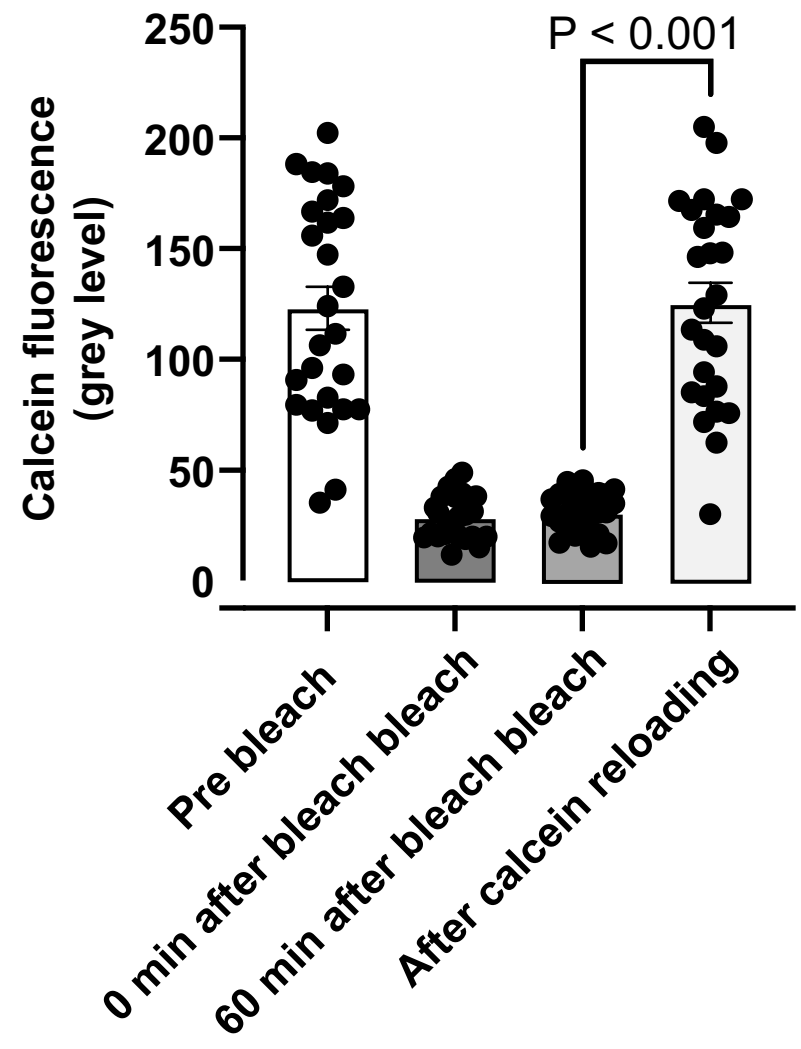

SUPPLEMENTARY FIGURE 5

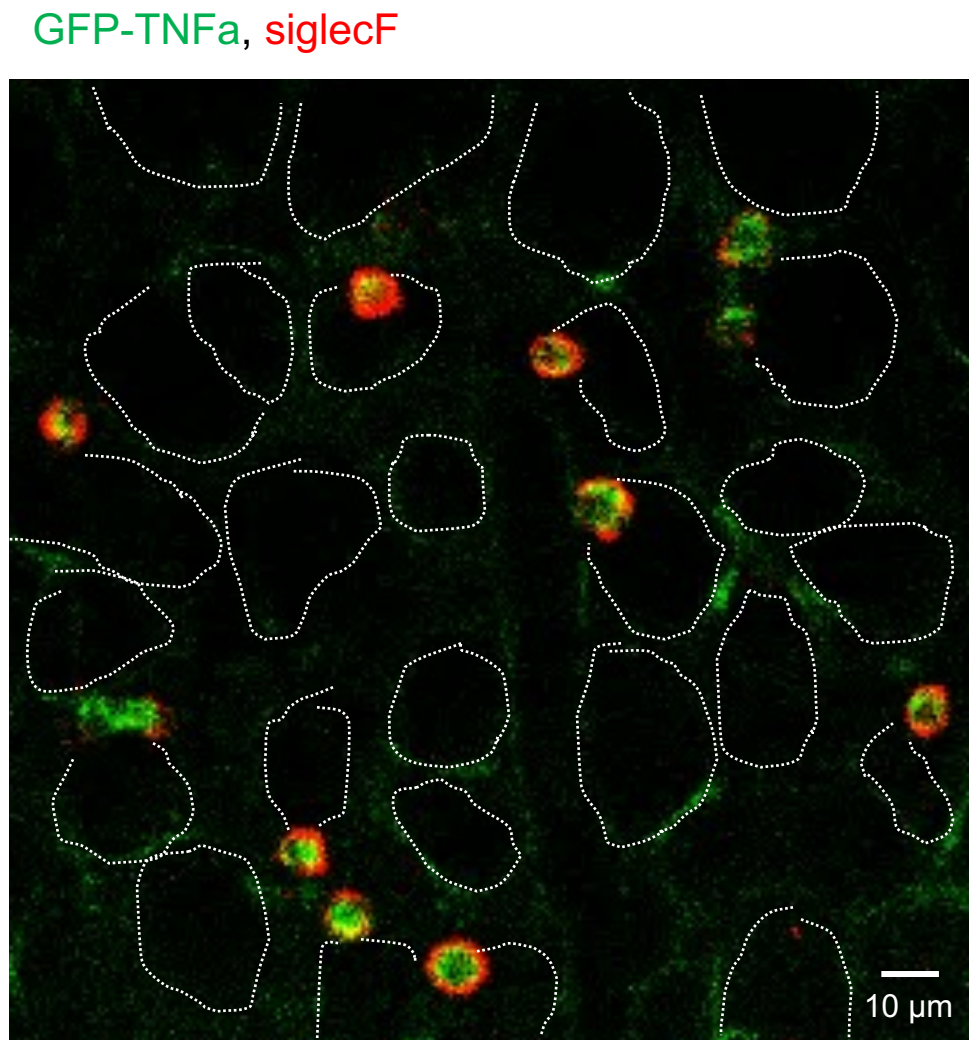

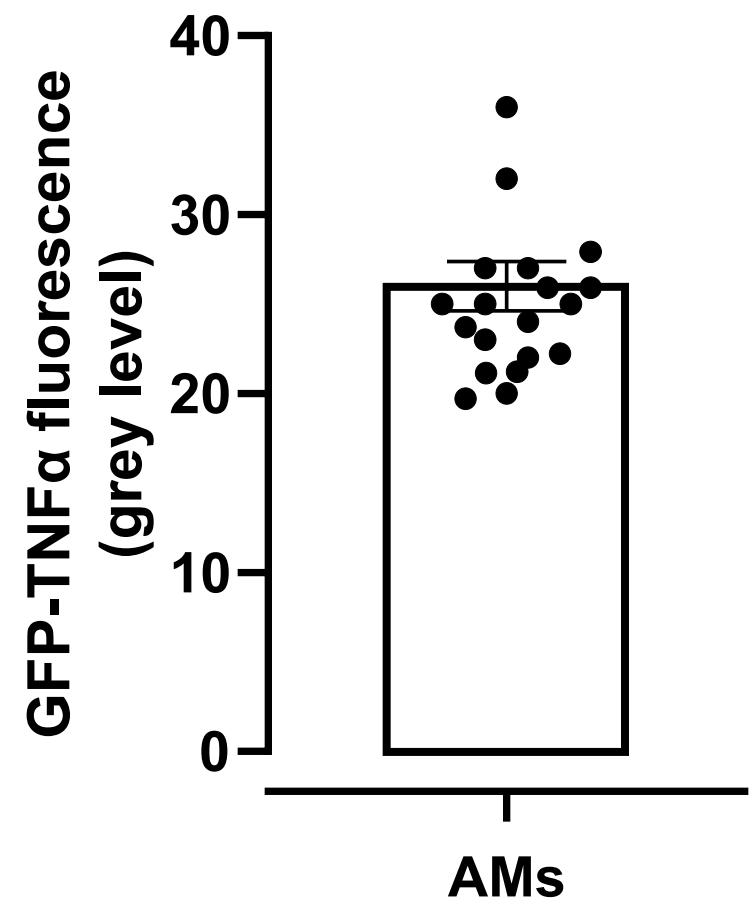

SUPPLEMENTARY FIGURE 6

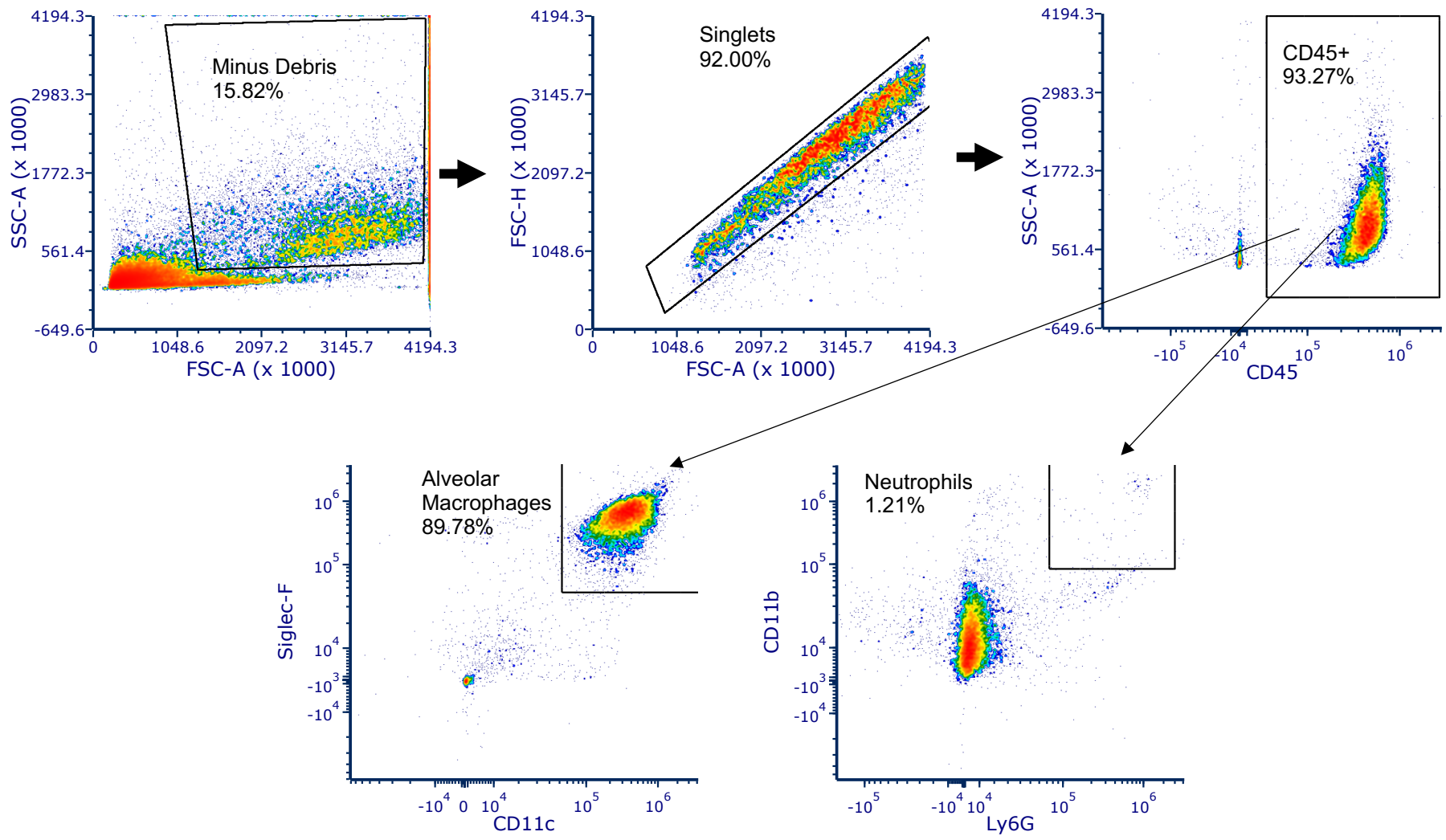

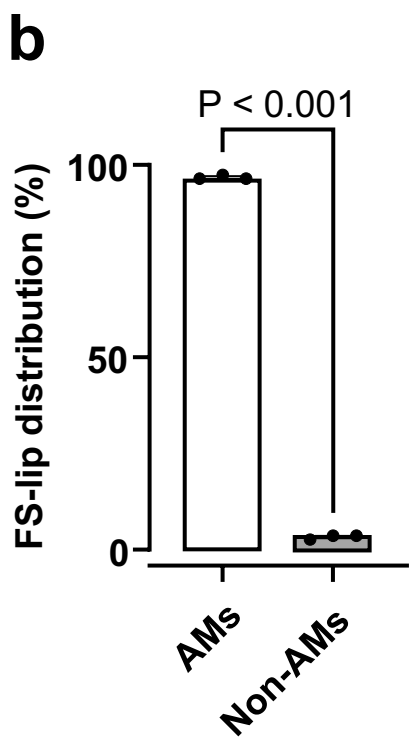

SUPPLEMENTARY TABLE 1

Name, Fluorescent Dye	Supplier	Catalogue No.	Stock Conc.	Final Conc.	Lot No.
CD45, Pacific Blue	Biolegend	103126	0.5 mg/ml	0.5 µg/ml	B314223
Ly-6G, Pe/Cy7	Biolegend	127618	0.2 mg/ml	0.2 µg/ml	B351626
F4/80, Pe/Cy7	Biologend	123113	0.2 mg/ml	0.2 µg/ml	B280918
CD11b, Pe/Cy5	Biolegend	101210	0.2 mg/ml	0.2 µg/ml	B260953
CD11c, APC	Biolegend	117310	0.2 mg/ml	0.2 µg/ml	B278343
SiglecF, PE	Biolegend	155506	0.2 mg/ml	0.2 µg/ml	B301117l
SiglecF, 488	Invitrogen	53-1702-80	0.2 mg/ml	0.2 µg/ml	2072850
TNFR1, Alexa Flour 633	AbD Serotec	MCA2350	10 mg/ml	40 µg/ml	n/a